Anderson Impurities In Edge States with Nonlinear and Dissipative Perturbations

Vinayak M Kulkarni [1 *], N. S. Vidhyadhiraja [1]

1 Theoretical Sciences Unit, Jawaharlal Nehru Centre for Advanced Scientific Research, Bangalore 560064, India.

* vmkphysimath@gmail.com

Abstract

A nontrivial renormalization of impurity problems shown by anisotropic and pseudochiral ($\mathcal{PC}$) interactions as dissipative perturbations. Using renormalization group (RG) analysis, Fock-space diagonalization, and relaxation-time calculations, we explore how nonlinear dispersion and potential scattering terms lead to exceptional points (EPs) and Hermiticity breaking in weak to intermediate interaction regimes. Inspired by Shnirman et al.Phys. Rev. A **50**, 3453, showed that cubic nonlinearity induces non-Hermiticity(NH), and more recently Nakai et al.Phys. Rev. A **109**, 144203 show sensitivity to perturbation in non-Hermitian(NH) problems using condition number analysis and Fike Bauer Theorem. Here we derive an effective Kondo model with emergent anisotropic Dzyaloshinskii-Moriya ($\mathcal{DM}$) interactions leading to the breaking of Hermiticity under perturbative RG. The RG analysis identifies new dissipative fixed points with a scaling collapse in spin relaxation time. The model exhibits an extended Lie group structure due to $\mathcal{PC}$-symmetric degrees of freedom, which reveal dissipative fixed points without renormalizing the invariant. Extending to a two-impurity Kondo model, we confirm that anisotropy is necessary for $\mathcal{PC}$ symmetry, and the RG equations show a "Sign Reversion" (SR) regime for anisotropic-Hermitian problems at critical nonlinear coupling J_{k^3}. Additionally, local Hamiltonians in Fock space display topological features at these dissipative fixed points.

1 Introduction

Non-Hermitian (NH) models have been extensively studied in open quantum systems [1,2], yet their role in closed condensed matter systems remains less explored. A particularly intriguing question is how interactions can induce NH degeneracies, such as exceptional points (EPs), within otherwise closed systems. While connections between EPs and Lindbladian dynamics have been established [3], the emergence of EPs due to many-body interactions remains an open challenge. In this work, we explore how anisotropic interactions in impurity models can lead to NH effects and EPs under perturbative renormalization.

Several mechanisms can introduce NH terms in condensed matter systems, including symmetry constraints and Lindbladian descriptions [4, 5]. Here, we focus on an alternative approach: nonlinear corrections to dispersion and impurity-bath interactions, which give rise to emergent anisotropic terms. Previous work by Shnirman et al. [6] demonstrated that nonlinear dispersion in the group velocity can introduce NH behavior via Bethe Ansatz solutions. More recently, Nakai et al. [7] used condition number analysis to study perturbation sensitivity in NH systems. Inspired by these results, we consider an impurity coupled to a chiral bath with nonlinear dispersion, leading to emergent NH effects.

Anisotropy plays a crucial role in NH impurity models, particularly in the context of potential scattering and dissipative interactions. Recent studies indicate that boundary conditions alone can induce openness in impurity models [8–10], much like the role of potential scattering in impurity-bath interactions. Additionally, inelastic scattering becomes significant when nonlinear perturbations are introduced into the bath. Experimentally, non-Hermitian transitions have been observed in condensed matter systems via spectroscopic measurements [11], and nonlinearity has been shown to control NH topological phase transitions [12]. In Kondo models, sign reversals in RG flows have been observed in NH contexts [4, 13, 14], with recent work highlighting causality violations in interacting and non-interacting NH systems [15, 16].

We further draw inspiration from anisotropic quantum Hall systems with C_4 symmetry [17–19], where strong interactions induce anisotropic features and non-equilibrium steady states. Extending these ideas, we examine impurity scattering in a bath with C_3 symmetry, leading to NH effects driven by anisotropy. Prior work has established that interaction-induced NH effects manifest in bound states, edge states, and flat bands [20]. Higher-order EPs have been observed in $\mathcal{PC}$-symmetric systems [21], with non-linear eigenvalue problems that produce auxiliary eigenvalues for small non-linear interactions [22]. Furthermore,EPs have been experimentally confirmed in real materials and synthetic systems [23, 24].

In this paper, we demonstrate that specific NH scattering processes become relevant in the weak-to-intermediate interaction regime of an anisotropic $\mathcal{DM}$ Kondo model. Using perturbative Poorman scaling with potential scattering, Fock-space diagonalization, and transport calculations, we identify novel dissipative fixed points.

We begin with a general model [25–27] describing a topological bath with nonlinear dispersion coupled to an interacting impurity. Projecting onto the singly occupied subspace of the impurity leads to an effective Hamiltonian with anisotropic interactions. Our analysis reveals that anisotropy and additional degrees of freedom give rise to emergent pseudo-chiral symmetry. Near the critical points of the RG flow, the system exhibits topological features in its spectrum, including EPs. Incorporating $\mathcal{PC}$-symmetric scattering terms leads to a Lie algebra structure connected to the conformal field theory (CFT) results of Pereira et al. [5], emphasizing the model's topological properties.

We then extend the model to a two-impurity Kondo (TIK) system. Our perturbative RG calculations reveal novel fixed points, supported by both analytical and numerical solutions of the RG equations. We explore the scaling behavior of impurity spin relaxation time and its relation to RG invariants.

The key result of this paper is that anisotropy, originating from nonlinear dispersion in the bath, leads to the breakdown of Hermiticity in the impurity-relevant regime under renormalization.

2 Model and Formalism

We begin with a bath model considered in the context of topological insulators [25], and the Hamiltonian reads as:

$$\hat{H} = \alpha k_{\parallel}^2 \mathbb{I} + \beta k_{\parallel}^3 \cos(3\theta)\sigma_z + i\lambda \hat{z} \cdot (\vec{k} \times \vec{\sigma}), \tag{1}$$

where $\vec{k} = k_x \hat{i} + k_y \hat{j} + k_{\parallel} \hat{k}$ and $\vec{\sigma} = \sigma_x \hat{i} + \sigma_y \hat{j} + \sigma_z \hat{k}$, with $\sigma_{x,y,z}$ being Pauli matrices. The parameters α, β, and λ correspond to quadratic, cubic, and linear couplings in the topological system, respectively. The second quantized form of the Hamiltonian for spinful fermions is $H = \sum_k \psi_k^\dagger \hat{H} \psi_k$. Where the basis vector is $\psi_k^\dagger = \begin{pmatrix} c_{k\uparrow}^\dagger & c_{k\downarrow}^\dagger \end{pmatrix}$. Introducing an impurity with on-site interaction generally regarded as the single impurity Anderson model (SIAM) and hybridization with the edge states leads to the Hamiltonian:

$$H_{\text{SIAM}} = \psi^\dagger \hat{H} \psi + H_d + \sum_{k\sigma} V_k (c_{k\sigma}^\dagger d_\sigma + \text{h.c.}), \tag{2}$$

where H_d is defined as $H_d = \sum_\sigma \epsilon_d d^\dagger_\sigma d_\sigma + U n_{d\uparrow} n_{d\downarrow}$.To simplify the bath Hamiltonian, we use the parametrization $k_x \pm i k_y = k_\| e^{\pm i\theta}$ and apply a k-dependent unitary operation on the bath operators, preserving canonical relations. This results in a nonlinear k-dependent coefficient as shown below,

$$\mathcal{U} = \frac{1}{\sqrt{\mathcal{N}}} \begin{pmatrix} e^{i\frac{\theta}{2}}\alpha_{k1} & -ie^{i\frac{\theta}{2}}\alpha_{k2} \\ e^{-i\frac{\theta}{2}}\alpha_{k2} & ie^{-i\frac{\theta}{2}}\alpha_{k1} \end{pmatrix} \tag{3}$$

In above equation 3 coefficients $\alpha_{k1} = \sqrt{\Delta + \beta k^3 \cos 3\theta}$ and $\alpha_{k2} = \sqrt{\Delta - \beta k^3 \cos 3\theta}$.And the normalization constant is $\mathcal{N} = |\alpha_{k1}|^2 + |\alpha_{k2}|^2 = \Delta$, where $\Delta = \sqrt{\beta^2 k^6 \cos^2 3\theta + \lambda^2 k^2} = \beta k^3 \gamma \cos 3\theta$, with $\gamma = \sqrt{1 + \frac{\lambda^2}{\beta^2 k^4 \cos^2 3\theta}}$. In the limit $\lambda \to 0$ or $\beta \to \infty$, the γ will tend to unity. In equation 3 choice for α_{k2} can be $\sqrt{\beta k^3 \cos 3\theta - \Delta}$ or $i\sqrt{\Delta - \beta k^3 \cos 3\theta}$. Both forms diagonalize the bath Hamiltonian having two chiral bands with the eigenenergies $\epsilon_{k\zeta} = \alpha k^2 + \zeta\Delta$ and it's eigenvalues are shown in figure 1.This non-interacting spectrum is similar to Rashba study [?] except from nonlinear term which serves as additional parameter to tune band touching to gapped phase in the bath.This unitary transformation rotates the bath operators as $\tilde{\psi}_k = \mathcal{U}_k \psi_k$. Such k-dependent operations are used in the case of Weyl multiplicity [28, 29] having different nonlinear dispersion as $(k_x \pm i k_y)^3$.Basis after rotation $\tilde{\psi} = \begin{pmatrix} c_{k+} \\ c_{k-} \end{pmatrix} = \mathcal{U}\psi$ can be shown as,

$$c_{k+} = \frac{1}{\sqrt{\beta\gamma k^3 \cos 3\theta}} \left(e^{-i\frac{\theta}{2}} \alpha_{k1} c_{k\uparrow} + e^{i\frac{\theta}{2}} \alpha_{k2} c_{k\downarrow} \right), c_{k-} = \frac{1}{\sqrt{\beta\gamma k^3 \cos 3\theta}} \left(ie^{i\frac{\theta}{2}} \alpha_{k2} c_{k\uparrow} - ie^{i\frac{\theta}{2}} \alpha_{k1} c_{k\downarrow} \right) \tag{4}$$

Using $\psi = \mathcal{U}^{-1}\tilde{\psi}$ to express the original spin basis in terms of these new chiral basis,

$$c_{k\uparrow} = \frac{1}{\sqrt{\beta\gamma k^3 \cos 3\theta}} \left(e^{i\frac{\theta}{2}} \alpha_{k1} c_{k+} - ie^{i\frac{\theta}{2}} \alpha_{k2} c_{k-} \right), c_{k\downarrow} = \frac{1}{\sqrt{\beta\gamma k^3 \cos 3\theta}} \left(e^{-i\frac{\theta}{2}} \alpha_{k2} c_{k+} + ie^{-i\frac{\theta}{2}} \alpha_{k1} c_{k-} \right) \tag{5}$$

In new basis the hybridization transforms as follows:

$$\begin{aligned} \tilde{H}^+_{hyb} &= \sum_{k\theta} \tilde{V}^\theta_k \left(e^{-i\frac{\theta}{2}} \alpha_{k1} c^\dagger_{k+} d_\uparrow + \text{h.c.} \right) + \sum_{k\theta} \tilde{V}^\theta_k \left(e^{i\frac{\theta}{2}} \alpha_{k2} c^\dagger_{k+} d_\downarrow + \text{h.c.} \right) \\ \tilde{H}^-_{hyb} &= \sum_{k\theta} \tilde{V}^\theta_k \left(ie^{-i\frac{\theta}{2}} \alpha_{k2} c^\dagger_{k-} d_\uparrow + \text{h.c.} \right) + \sum_{k\theta} \tilde{V}^\theta_k \left(-ie^{i\frac{\theta}{2}} \alpha_{k1} c^\dagger_{k-} d_\downarrow + \text{h.c.} \right) \end{aligned} \tag{6}$$

In above equation 6 $\tilde{V}^\theta_k = \frac{V_k}{\sqrt{\beta\gamma k^3 \cos 3\theta}}$ has k, θ dependence. A square root momentum dependent hybridization found in Rashba coupling studies [30–33].After the unitary rotation, we obtain the renormalized SIAM as follows:

$$\tilde{H} = \sum_{k\zeta} \epsilon_{k\zeta} c^\dagger_{k\zeta} c_{k\zeta} + H_d + \tilde{H}^+_{hyb} + \tilde{H}^-_{hyb} \tag{7}$$

The above equation 7 satisfies the pseudo-chirality, as $\eta\tilde{H}\eta^{-1} = -\tilde{H}^\dagger$, when the couplings are complex-valued. This symmetry for Hermitian problem can be written as $\{\tilde{H}, \eta\} = 0$ the η is constructed as $\sigma_x \otimes \sigma_x$ for $U = 0$ in matrix form we can also construct in operator form [?] as $\psi^\dagger \eta \psi$ where $\psi^\dagger = \begin{pmatrix} c^\dagger_+ & c^\dagger_- & d^\dagger_\uparrow & d^\dagger_\downarrow \end{pmatrix}$.Generally the $\mathcal{PT}$ - symmetry is associated with the

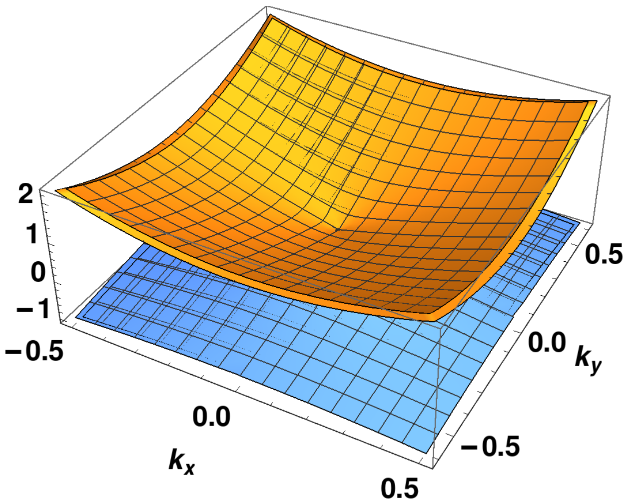

Figure 1: The eigenvalues of the diagonalized model in equation 1 around the low k points represent the emergent chiral bands. In this case, we set $\beta = 0.3$, $\lambda = 1.0$, and $\theta = \frac{\pi}{3}$. We observed that larger β values flatten the bands.

NH transitions but in presence of topology and NH lead to additional symmetry classes [34] as follows,

$$\begin{aligned} \eta H \eta^{-1} &= H^{\dagger} \text{ for } \mathcal{PT} \text{ symmetry} \\ \eta H \eta^{-1} &= -H^{\dagger} \text{ for } \mathcal{PC} \text{ symmetry} \end{aligned} \tag{8}$$

These above symmetries parity-time($\mathcal{PT}$) and $\mathcal{PC}$ will be written as $[H, \eta] = 0$ and $\{H, \eta\} = 0$, when $H = H^{\dagger}$. These observations will guide us on how the formation of exceptional points occurs when couplings are complex-valued without altering the symmetry.

3 Effective Model Derivation And Poorman Scaling

To project this model in equation 7 onto the impurity subspace, we use projection operator method [35]. The projection operators are defined as $P_0 = (1-n_{\uparrow})(1-n_{\downarrow})$, $P_1 = n_{\uparrow}(1-n_{\downarrow}) + n_{\downarrow}(1-n_{\uparrow})$, and$P_2 = n_{\uparrow} n_{\downarrow}$ for unoccupied, singly occupied, and doubly occupied states, respectively. Using these projections, we derive the components of the effective model as $H_{\eta\eta'} = P_{\eta} H P_{\eta'}$ which is detailed in Appendix A.The emergent quantum numbers $\zeta = \pm$ represent chiral bands in the effective model.

$$H^{\eta}_{eff} = H_{\eta\eta} + \sum_{\substack{\eta' \neq \eta = 0,1,2 \\ \zeta, \zeta' = \pm}} H^{\zeta}_{\eta\eta'} \frac{1}{E - H_{\eta'\eta'}} H^{\zeta'}_{\eta'\eta} \tag{9}$$

The singly occupied subspace Hamiltonian is the low-energy effective model for the Kondo regime. We show here for such a topological bath one gets an effective model which has emergent anisotropic $\mathcal{DM}$ interactions.We adopt a specific convention for representing couplings. We utilize vector notation to denote couplings, while pseudo-spin of bath operators are represented using bold symbols. This notation allows us to distinguish between different types of operators.

$$H^{1}_{eff} = H_0 + \sum_{kk'} J_0 s \cdot \mathbf{S}_{kk'} + i \sum_{kk'} \vec{J}_{k^3} \cdot (s \times \mathbf{S}_{kk'}) + i \sum_{kk'} \vec{J}_k \cdot (s \times \mathbf{S}_{kk'}) \tag{10}$$

In equation 10,$H_0 = \sum_{k\zeta} \epsilon_{k\zeta} c^{\dagger}_{k\zeta} c_{k\zeta}$ and the operator $\boldsymbol{S}_{kk'}$ represents the Abrikosov pseudo-spin for conduction electrons, while s corresponds to the impurity spin.The couplings are denoted as $J_0 = (\alpha_{k1}\alpha_{k'1} + \alpha_{k2}\alpha_{k'2})M^{\theta,\theta'}_{kk'\zeta}$, $\vec{J}_{k^3} = (\alpha_{k1}\alpha_{k'1} - \alpha_{k2}\alpha_{k'2})M^{\theta,\theta'}_{kk'\zeta}\hat{z}$ and $\vec{J}_k = \alpha_{k1}\alpha_{k'2}M^{\theta,\theta'}_{kk'\zeta}(\hat{x}+\hat{y})$. Here, $M^{\theta\theta'}_{kk'\zeta} = \tilde{V}^{\theta}_{k}\tilde{V}^{\theta'}_{k'}\left(\frac{1}{\epsilon_{k'\zeta}-\epsilon_d} + \frac{1}{\epsilon_d + U - \epsilon_{k\zeta}}\right)$ and $\tilde{V}^{\theta'}_{k'} = \frac{V_{k'}}{\sqrt{\beta\gamma(k')^3 \cos 3\theta'}}$.The matrix elements in this problem in general depend on polar angles and momenta are derived in Appendix A. The nonlinear dispersion introduces cross-product terms in z component and linear term will introduce x,y components of $\mathcal{DM}$.Poorman RG will yield following equations,

$$\frac{dJ_0}{dl} = J_0^2 + J_{k^3}J_k + J_{k^3}^2 + J_k^2, \frac{dJ_{k^3}}{dl} = J_k^2 + J_0 J_{k^3}, \frac{dJ_k}{dl} = J_0 J_k \tag{11}$$

The appendix B contains a detailed derivation and the complete solution to the RG equations 11. One of the solutions, obtained by eliminating J_0 in $\frac{dJ_k}{dl}$ and $\frac{dJ_{k3}}{dl}$ equations, is given by the equation $J_k^2 - J_k = mJ_{k^3}$, where m can be a positive or negative value. The roots of this solution are expressed as $J_k = \frac{1}{2} \pm \frac{1}{2}\sqrt{1 + 4mJ_{k^3}}$. In the low-energy effective model, it plays a significant role in causing exceptional points, which will be discussed in detail in the subsequent section, along with the diagonalization.

4 Emergence Of Complex Solution

We performed poorman RG on Hamiltonian as in the equation 11 and found the invariants $\tilde{J}_0$, $\tilde{J}_k$ as shown in Appendix C.Here we analyse the local Hamiltonian symmetry properties and its eigenvalue spectrum using the RG invariants for couplings and varying the J_{k^3}.

$$\tilde{H} = \sum_{kk'} \tilde{J}_0 s \cdot \boldsymbol{S}_{kk'} + i \sum_{kk'} \vec{\tilde{J}}_{k^3} \cdot (s \times \boldsymbol{S}_{kk'}) + i \sum_{kk'} \vec{\tilde{J}}_k \cdot (s \times \boldsymbol{S}_{kk'}) \tag{12}$$

In order to show the effective model above exhibits pseudo-chiral symmetry, we can write the local Hamiltonian at $k = 0$ as follows:

$$\begin{aligned} \hat{\tilde{H}} = \tilde{J}_0(\sigma_z \otimes \boldsymbol{\sigma}_z + \sigma^+ \otimes \boldsymbol{\sigma}^- + \sigma^- \otimes \boldsymbol{\sigma}^+) + i\tilde{J}_{k^3}(\sigma_x \otimes \boldsymbol{\sigma}_y - \boldsymbol{\sigma}_y \otimes \sigma_x) \\ + i\tilde{J}_k(\sigma_y \otimes \boldsymbol{\sigma}_z - \boldsymbol{\sigma}_z \otimes \sigma_y) + i\tilde{J}_k(\sigma_x \otimes \boldsymbol{\sigma}_z - \boldsymbol{\sigma}_z \otimes \sigma_x) \end{aligned} \tag{13}$$

We can construct the ket vector for the above Hamiltonian as $(|\uparrow\uparrow\rangle, |\uparrow\downarrow\rangle, |\downarrow\uparrow\rangle, |\downarrow\downarrow\rangle)$. For such a state, we can show the metric operator as the following:

$$\eta = \begin{pmatrix} 0 & 0 & 0 & 1 \\ 0 & 0 & 1 & 0 \\ 0 & 1 & 0 & 0 \\ 1 & 0 & 0 & 0 \end{pmatrix} \tag{14}$$

In the above equation 13 the block symbol is for the bath spin and rest are impurity spin operators to distinguish between the two.The chiral symmetry operator can be generalized to n-dimensional matrices [36], is $\eta = \boldsymbol{\sigma}_x \otimes \sigma_x$. This metric satisfies $\eta\tilde{H}\eta^{-1} = -\tilde{H}^{\dagger}$, indicating pseudo-chiral symmetry [34] this inherent property become very crucial after adding the potential scattering terms which is eloborated in section V. For Hermitian matrix this symmetry will be $\{\hat{H}, \eta\} = 0$. This symmetry also exists when $J_0 \to 0$ and even if all couplings are real-valued. Each of the states can be represented as follows:

$$\langle\uparrow\uparrow| = \begin{pmatrix}1 & 0 & 1 & 0\end{pmatrix}, \langle\uparrow\downarrow| = \begin{pmatrix}1 & 0 & 0 & 1\end{pmatrix}, \langle\downarrow\uparrow| = \begin{pmatrix}0 & 1 & 1 & 0\end{pmatrix}, \langle\downarrow\downarrow| = \begin{pmatrix}0 & 1 & 0 & 1\end{pmatrix} \tag{15}$$

So it can be readily seen the operations as $\eta|\uparrow\uparrow\rangle \rightarrow |\downarrow\downarrow\rangle$, $\eta|\uparrow\downarrow\rangle \rightarrow |\downarrow\uparrow\rangle$, $\eta|\uparrow\downarrow\rangle \rightarrow |\downarrow\uparrow\rangle$ and $\eta|\downarrow\downarrow\rangle \rightarrow |\uparrow\uparrow\rangle$.

$$\hat{\hat{H}} = \begin{pmatrix} J_0 & -J_k e^{-i\frac{\pi}{4}} & J_k e^{-i\frac{\pi}{4}} & 0 \\ -J_k e^{i\frac{\pi}{4}} & -J_0 & 2iJ_{k^3} + J_0 & -J_k e^{-i\frac{\pi}{4}} \\ J_k e^{i\frac{\pi}{4}} & -2iJ_{k^3} + J_0 & -J_0 & J_k e^{-i\frac{\pi}{4}} \\ 0 & -J_k e^{i\frac{\pi}{4}} & J_k e^{-i\frac{\pi}{4}} & J_0 \end{pmatrix} \tag{16}$$

The above matrix has some specific properties due to the anisotropic $\mathcal{DM}$ interaction,

$$\begin{aligned} \eta_{\sigma_z\otimes\sigma_z}\hat{H}\eta^{-1}_{\sigma_z\otimes\sigma_z} &= H \text{ for } J_k \rightarrow -J_k \\ \eta_{\sigma_y\otimes\sigma_y}\hat{H}\eta^{-1}_{\sigma_y\otimes\sigma_y} &= H \text{ for } J_{k^3} \rightarrow 0 \end{aligned} \tag{17}$$

In our analysis, we examine the eigenvalues of the spin Hamiltonian defined in equation 16 within the $(1,1)$ occupancy sector. This is represented in figures 2 and 3. We observe the emergence of complex eigenvalues and the formation of exceptional points due to perturbative RG. This phenomenon is also evident in the one-loop and Poorman equations in non-Hermitian scenarios [4,5]. Here, we present numerical evidence of the spectral properties at these fixed points.

Using Fock-space diagonalization with $\tilde{J}_k = \frac{1}{2} \pm \frac{1}{2}\sqrt{1+4mJ_{k^3}}$ in the single occupancy sector(SS), we find that for $J_{k^3} < |0.5|$, the eigenvalues follow hyperbolic trajectories typical of the conventional Kondo regime. However, for values greater than the critical value, topological transitions occur in the spectrum. In the resonant level scenario depicted in figure 3, exceptional points emerge for large m values.

As J_0 increases, the disappearance of the Dirac cone indicates the emergence of a spectral gap. This observation underscores the role of the RG invariant $J_k = \frac{1}{2} \pm \frac{1}{2}\sqrt{1+4mJ_{k^3}}$ in shaping the impurity spectrum. This invariant is crucial for the appearance of coalescing points in the spectrum, revealing the complex interplay between coupling parameters and their renormalization under RG flow. These coalescing points vanish as $J_0 \rightarrow \infty$.

4.1 Condition Number In Fock Space

The condition number [37] $\kappa(A)$ of matrix A is defined as $\kappa(A) = \frac{|\lambda_{max}|}{|\lambda_{min}|}$, where λ_{max} and λ_{min} correspond to the highest and lowest eigenvalues. This number is associated with error in measurement, sensitivity, and the singular spectrum of real and complex-valued matrices. We illustrate this number in plots 4 and 5 for one and two impurities for local Hamiltonian in spin Fock space. The sensitivity of the models with J_{k^3} versus K type of $\mathcal{DM}$ interactions is also depicted. The defectiveness in diagonalization is attributed to eigenvector becoming parallel and loss of orthogonality indicating exceptional points. However, the conclusion made here is based on the local Hamiltonian in sector one fock space, hence this is relevant to the dissipation in this subsystem and does not translate to full many-body systems. Note that dissipation in large N systems generally shown to be relevant for local system, since larger systems always tend to equilibrate. Recently the perturbation sensitivity to NH systems [7] has been shown using condition number analysis.

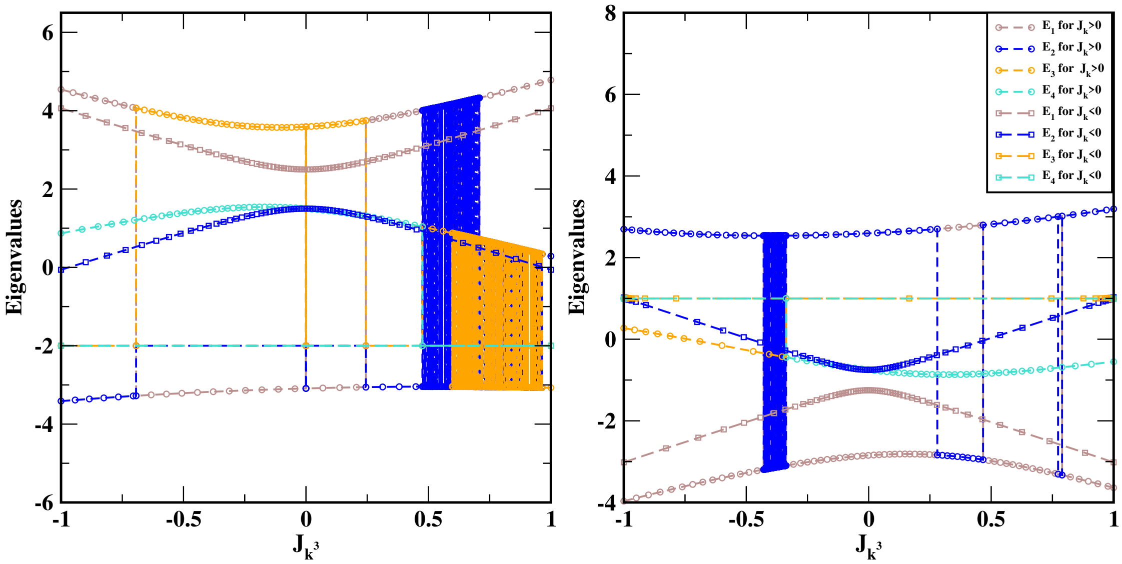

Figure 2: The eigenvalues of the model (equation 16) with $J_0 = -2.0$ (above) and $J_0 = 1.0$ (below), along with the RG invariant $m = \pm 0.01$. For small values of m and two roots denoted as $J_0 < 0, J_0 > 0$, the eigenvalues are denoted from E_1 to E_4 for corresponding RG root. Topological transitions occur at $J_{k^3} = \pm 0.5$ and around $J_{k^3} = 0.75$. At smaller values of m, there will be small imaginary weights in the eigenvalues, but no exceptional points. These topological points remain at higher values of m, but the spectrum will be gapped due to higher J_0 values.

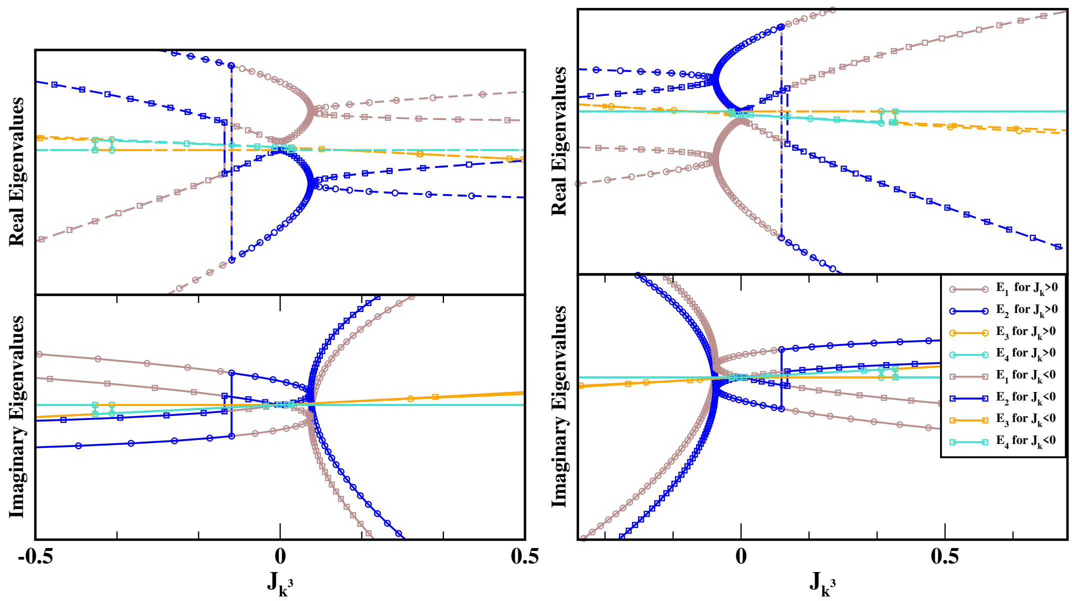

Figure 3: Eigenvalues of the equation 16 for resonant level cases(small J_0).For $J_0 = \pm 0.1$ and the RG invariant $m = \pm 4.0$. The labels E_1 to E_4 denote four different eigenvalues for positive and negative RG invariants, respectively. A Dirac cone appears in the impurity spectrum due to the topological properties of the local Hamiltonian. Larger values of m are required to observe exceptional points, and the gap in the spectrum widens with increasing J_0.

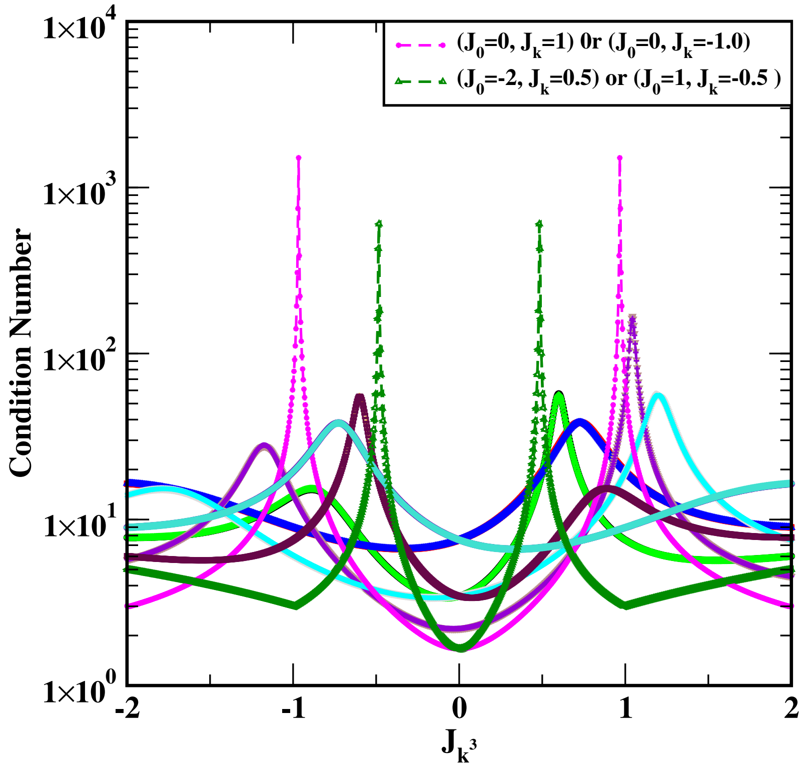

Figure 4: Variation of the condition number with anisotropic $\mathcal{DM}$ coupling J_{k^3} in the model in equation 13, using Fock-space diagonalization in the SS of the one-impurity problem. Diverging cusp-like points indicate high condition numbers denoted in graph implies defects in diagonalization found figure2.

5 Renormalization With Potential Scattering

We analyze the coefficients of effective model and construct the regular hexagonal boundaries of the bath as shown in figure 6.The spin-spin interaction model resembles the structure in work [5] after including potential scattering terms. Our goal is to examine whether the invariant responsible for coalescence (Exceptional Point, EP) undergoes renormalization or remains unrenormalized with the inclusion of non-Hermitian terms, particularly at third-order RG corrections. Complex-valued potential scattering is essential for obtaining fixed points in the flow, corresponding to ground state topological transitions in the eigenvalue spectrum of the model. The effective model with scattering terms can be expressed as follows:

$$H'_{eff} = H_0 + \sum_{kk'} J_0 s\cdot\psi^\dagger(\Sigma)\psi + i\sum_{kk'} \vec{J}_{k^3}^{0,0}\cdot(s\times\psi^\dagger(\Sigma)\psi) + i\sum_{kk'} \vec{J}_{k}^{(0,0)}\cdot(s\times\psi^\dagger(\Sigma)\psi) + H_{pot} \tag{18}$$

Where we add the $\mathcal{PC}$-symmetric potential scattering terms as shown in the figure 6 and represented as H_{pot} can be written as following,

$$H_{pot} = \sum_{kk'}\left(\vec{J}_{k^3}^{\frac{2\pi}{3},-\frac{\pi}{3}} + \vec{J}_{k}^{\frac{2\pi}{3},-\frac{\pi}{3}}\right)\cdot(s\times\psi^\dagger(\Gamma)\psi) - \sum_{kk'}\left(\vec{J}_{k^3}^{\pm\frac{2\pi}{3},\pm\frac{\pi}{3}} + \vec{J}_{k}^{\pm\frac{2\pi}{3},\pm\frac{\pi}{3}}\right)\cdot(s\times\psi^\dagger(\Omega)\psi) \tag{19}$$

Essentially, added degrees of freedom are $\psi^\dagger = \left(c^\dagger_{k\frac{2\pi}{3}+},\ c^\dagger_{k\frac{\pi}{3}-},\ c^\dagger_{-k-\frac{2\pi}{3}+},\ c^\dagger_{-k-\frac{\pi}{3}-}\right)$ needed to achieve the generalized Pauli matrices or the block structure of the Kondo problem and it is detailed in Appendix B3 we have shown by expanding the above model in detail to derive the RG

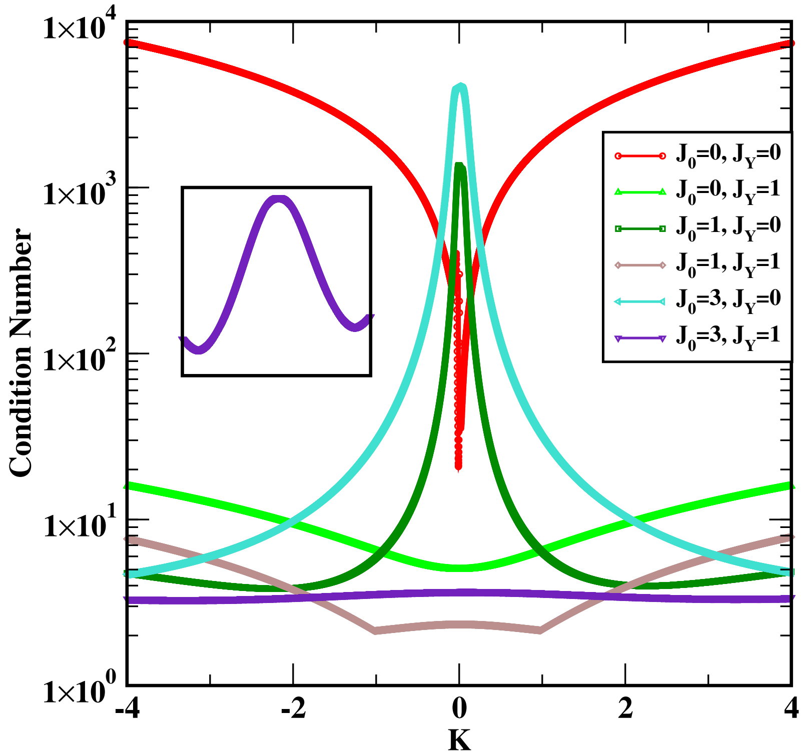

Figure 5: Variation of condition numbers in Fock space of the two-impurity model given in equation 23,and they show that the model is well conditioned for most values of K, except when K is 0. However, high condition numbers occur when the anisotropic coupling is non-zero, indicating that the model is not defective when J_{k^3} and J_k couplings are absent.

equations and those are plotted in the figure 7. We used the simplified notations for the couplings as $\left(J_0, J_{k^3}^{0,0}, J_{k^3}^{\pm\frac{2\pi}{3},\pm\frac{\pi}{3}}, J_{k^3}^{\frac{2\pi}{3},-\frac{\pi}{3}}, J_k^{(0,0)}, J_k^{\pm\frac{2\pi}{3},\pm\frac{\pi}{3}}, J_k^{\frac{2\pi}{3},-\frac{\pi}{3}}\right)$ into $\left(J_0, J_{k^3}, g_{1k^3}, g_{2k^3}, J_k, g_{1k}, g_{2k}\right)$.

6 Generalization to Two Impurities

We extend our model to a two-impurity Kondo system, incorporating direct spin-spin coupling and an isotropic $\mathcal{DM}$ interaction between impurities. Similar interactions have been studied in double quantum dots with spin-orbit coupling [38], where the $\mathcal{DM}$ term is restricted to the Y-component for baths with linear dispersion. Here, we analyze the renormalization of anisotropic versus isotropic interactions.

6.1 Effective Hamiltonian and Renormalization Group Equations

The effective spin Hamiltonian takes the form:

$$H_{\text{eff}} = H_0 + \sum_{kk'} J_0 s_\alpha \cdot \mathbf{S}_{kk'} + i \sum_{kk'\zeta} \vec{J}_{k^3} \cdot (s_\alpha \times \mathbf{S}_{kk'}) + i \sum_{kk'\zeta} \vec{J}_k \cdot (s_\alpha \times \mathbf{S}_{kk'}) + J_Y s_1 \cdot s_2 + i\vec{K} \cdot (s_1 \times s_2), \tag{20}$$

where $H_0 = \sum_{k\zeta} \epsilon_{k\zeta} c_{k\zeta}^\dagger c_{k\zeta}$ is the kinetic energy term, J_Y represents the direct coupling between impurities, and K denotes the impurity $\mathcal{DM}$ interaction. The bold symbols denote spinor vectors, as previously defined.

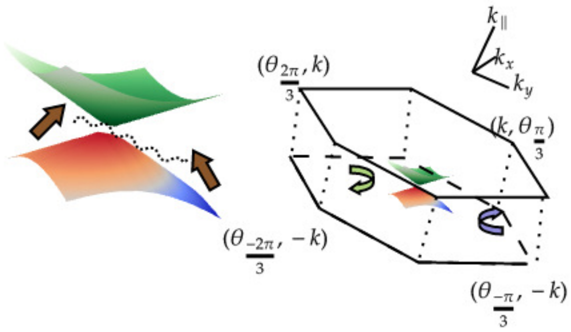

Figure 6: Left schematic representing two Anderson impurities in the edge states of the bath. Right one is regular hexagonal cell of bath to incorporate $\mathcal{PC}$ symmetric potential scattering terms. The left and right scatterers are depicted with green and blue arrows, respectively. Here, $k_{\parallel} \to k$, $\sqrt{k_x^2+k_y^2} \to k$ and $\theta \to \tan^{-1}\frac{k_y}{k_x}$. For derivations, see equations from 3 to 5. Electron and hole scatterings for (k,θ) to $(-k,\theta')$ are represented around the Dirac cone.Note that k is modulus of the vector and only its direction will decide the sign of momenta of hole or electron.

Since the generalized problem introduces multiple couplings, we restrict our analysis to the one-loop RG equations:

$$\begin{aligned}
\frac{dJ_0}{dl} &= J_0^2 + J_{k^3}J_k + J_{k^3}^2 + J_k^2 + J_Y J_0 + K J_0, \\
\frac{dJ_{k^3}}{dl} &= J_k^2 + J_0 J_{k^3} + J_Y J_{k^3} + J_Y J_k + K J_{k^3}, \\
\frac{dJ_k}{dl} &= J_0 J_k + J_Y J_{k^3} + J_Y J_k + K J_k, \\
\frac{dJ_Y}{dl} &= J_Y^2 + K^2 + J_0^2 + J_{k^3}J_k + J_k^2 + J_{k^3}^2, \\
\frac{dK}{dl} &= K^2 + K J_Y + J_{k^3}J_k.
\end{aligned} \tag{21}$$

Solutions to these equations, in various limiting cases, are detailed in the Appendix. The vanishing of the beta functions for Kondo destruction is analyzed within the odd-even coupling framework [39,40]. Given our focus on nonlinear couplings J_k, J_{k^3}, we investigate anomalous contributions to spin relaxation time and the fixed points governing these couplings.

6.2 Eigenspectrum and Fixed Points

To further understand the connection between RG fixed points and the eigenspectrum, we construct the three-spin Fock space representation for the two-impurity system. The effective Hamiltonian in this basis is:

$$\tilde{H}_{2\mathrm{imp}} = \sum_{kk'} \tilde{J}_0 s_\alpha \cdot \mathbf{S}_{kk'} + i\sum_{kk'\alpha} \vec{\tilde{J}}_{k^3} \cdot (s_\alpha \times \mathbf{S}_{kk'}) + i\sum_{kk'\alpha} \vec{\tilde{J}}_k \cdot (s_\alpha \times \mathbf{S}_{kk'}) + \tilde{J}_Y s_1 \cdot s_2 + i\vec{\tilde{K}} \cdot (s_1 \times s_2). \tag{22}$$

Here, α indexes the two impurities. The Fock space representation in the symmetric sector (SS) is given by:

$$\psi^\dagger = (|\uparrow\uparrow\uparrow\rangle, |\uparrow\uparrow\downarrow\rangle, |\uparrow\downarrow\uparrow\rangle, |\downarrow\uparrow\uparrow\rangle, |\uparrow\downarrow\downarrow\rangle, |\downarrow\downarrow\uparrow\rangle, |\downarrow\uparrow\downarrow\rangle, |\downarrow\downarrow\downarrow\rangle)$$

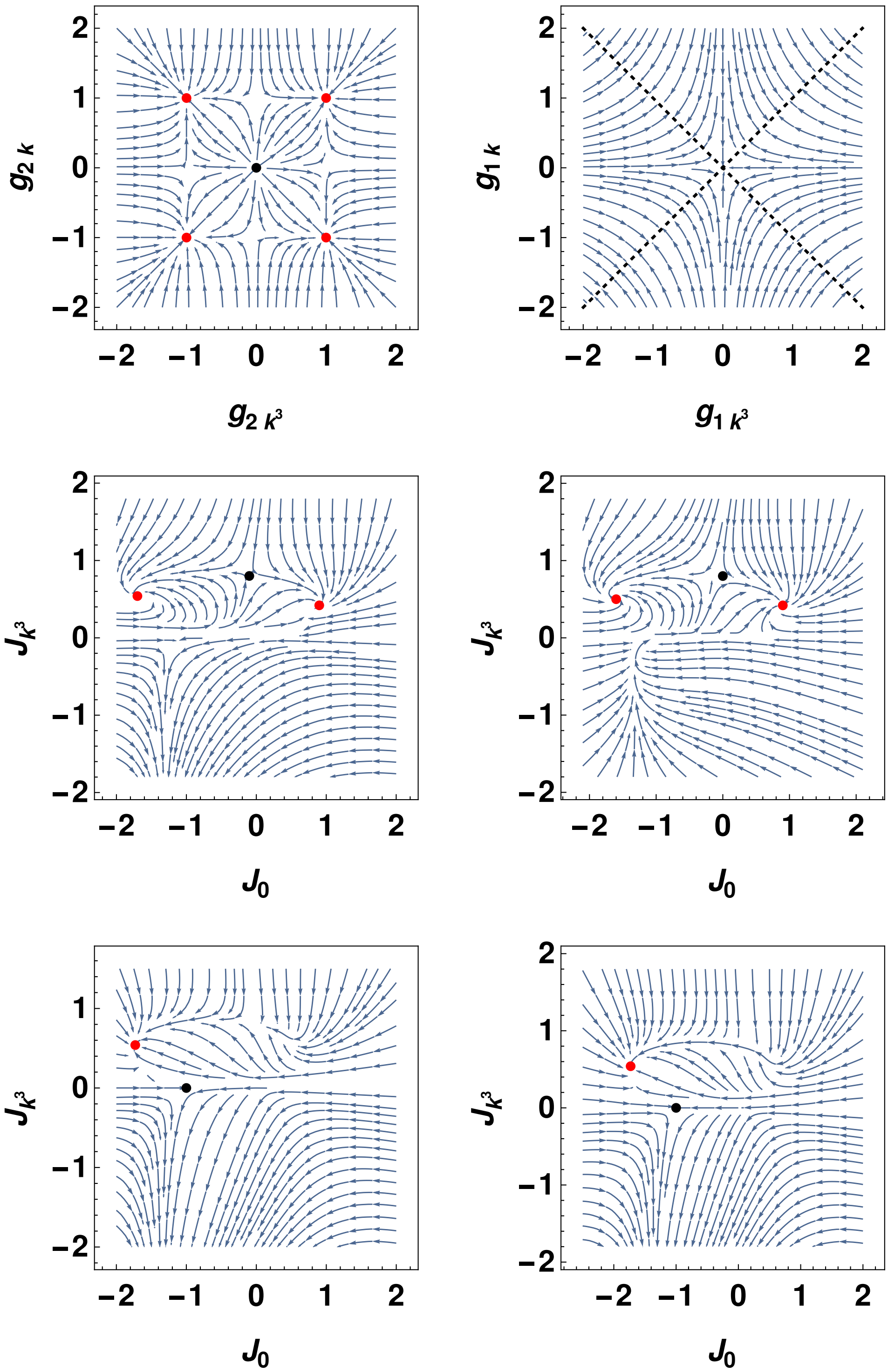

Figure 7: In these figures, we show the RG flow using the fixed values $g_{1k} = g_{1k^3} = 1$, which is invariant derived in the appendix B. Throughout our calculations, we use $J_{1k} = \frac{1}{2} \pm \frac{1}{2}\sqrt{1 + 4mJ_{1k^3}}$ alongside setting $m = -4$. The top row of the plots represents potential scattering, and the second row shows the real and imaginary parts of (J_{1k}) in both RG equations in x and y axes, where the notation (R^+, R^+) and $(R^+ I^+)$ denotes the real and imaginary parts on the x and y axes, respectively. Similarly, the third row is (I^-, R^-) and (I^-, I^-). We observe at least two fixed points (FP) and two spiral points(SP) in the second row, while the third row shows one SP and one marginal point. The dotted lines in the second plot of the first row represent a family of FPs.The EP signatures figure 3 in RG flow can be observed here as parallel arrows at small J_0 and J_{k^3} values, representing unstable solutions.At these SP we found topological transitions in figures2 and high condition numbers in figure 4 for $J_{k^3} = 0.5$.

The Hamiltonian is then expressed as:

$$\hat{\tilde{H}}_{2\mathrm{imp}} = \langle\psi|\tilde{H}_{2\mathrm{imp}}|\psi\rangle. \tag{23}$$

Expanding in matrix form, we analyze the symmetry properties of $\hat{\tilde{H}}_{2\mathrm{imp}}$. Constructing the metric operator $\hat{\eta} = \sigma_x \otimes \sigma_x \otimes \sigma_x$ as in Ref. [36], we verify its $\mathcal{PC}$ symmetry, expressed as:

$$\hat{\eta}\hat{H}\hat{\eta}^\dagger = -\hat{H}^\dagger.$$

We demonstrate that anisotropic $\mathcal{DM}$-interaction is necessary to satisfy this condition, specifically requiring $J_{k^3} \neq 0$. The Hamiltonian lacks $\mathcal{PC}$ symmetry when $J_{k^3} = 0$.

The full Hamiltonian matrix is given by:

$$\hat{\tilde{H}} = \begin{pmatrix}
2J_0 + J_Y & -e^{i\frac{\pi}{4}}J_{Kp} & 0 & 0 & e^{i\frac{\pi}{4}}J_{Kp} & 0 & 0 & 0 \\
-e^{-i\frac{\pi}{4}}J_{Kp} & -J_Y & 4J_{0p} & -2e^{i\frac{\pi}{4}}J_k & 4J_{Yp} & e^{i\frac{\pi}{4}}J_{Km} & 0 & 0 \\
0 & 4J_{0m} & -2J_0 + J_Y & e^{i\frac{\pi}{4}}J_{Km} & 4J_{0p} & 0 & -e^{i\frac{\pi}{4}}J_{Km} & 0 \\
0 & -2e^{-i\frac{\pi}{4}}J_k & e^{-i\frac{\pi}{4}}J_{Km} & -J_y & 0 & 4J_{0p} & 4J_{Yp} & -e^{i\frac{\pi}{4}}J_{Kp} \\
e^{-i\frac{\pi}{4}}J_{Kp} & 4J_{Ym} & 4J_{0m} & 0 & -J_y & -e^{i\frac{\pi}{4}}J_{Km} & -2e^{i\frac{\pi}{4}}J_k & 0 \\
0 & e^{-i\frac{\pi}{4}}J_{Km} & 0 & 4J_{0m} & -e^{-i\frac{\pi}{4}}J_{Km} & -2J_0 + J_y & 4J_{0p} & 0 \\
0 & 0 & -e^{-i\frac{\pi}{4}}J_{Km} & 4J_{Ym} & -2e^{-i\frac{\pi}{4}}J_k & 4J_{0m} & -J_y & e^{i\frac{\pi}{4}}J_{Kp} \\
0 & 0 & 0 & -e^{-i\frac{\pi}{4}}J_{Kp} & 0 & 0 & e^{-i\frac{\pi}{4}}J_{Kp} & 2J_0 + J_y
\end{pmatrix}$$

where we define the reduced notations $J_{Kp} = J_k + K$, $J_{Km} = J_k - K$, and analogous expressions for J_0 and J_Y.

7 Solutions for RG ODE

We calculated numerical solutions for the set of equations 21 and plotted them around the fixed points as initial conditions for the RG ODE. The results are shown in Figure 8. These solutions are restricted to real values, and we observe the renormalization of J_{k^3} and J_k in agreement with our analytical findings. In the next section, we analyze the general solutions around the dissipative fixed points.

7.1 RG Equations: Zeros and Poles Analysis

We analyze the RG ODEs by extending the solutions into the complex plane, treating them as RG beta functions [14]. These beta functions typically exhibit a single-peak structure at fixed points. Previous studies [4, 5, 14] indicate that complex fixed points exhibit unique features, including RG reversion.

Extending this concept, we observe that the peak structure in the imaginary part of the beta function undergoes a sign reversal. This behavior is illustrated in Figure 9, where spiral fixed points (SPs) can be identified through these features, which are characteristic of this type of dissipation.

Other features in the RG beta functions, such as zero crossings or the absence of a single-peak structure, are associated with unstable points. A more detailed quantitative analysis is required to classify the different types of fixed points. The analysis presented here remains robust across different methodological approaches.

Consistent results from both conformal field theory (CFT) and the renormalization group (RG) equations suggest that both approaches capture the essential physics of the problem and provide complementary insights.

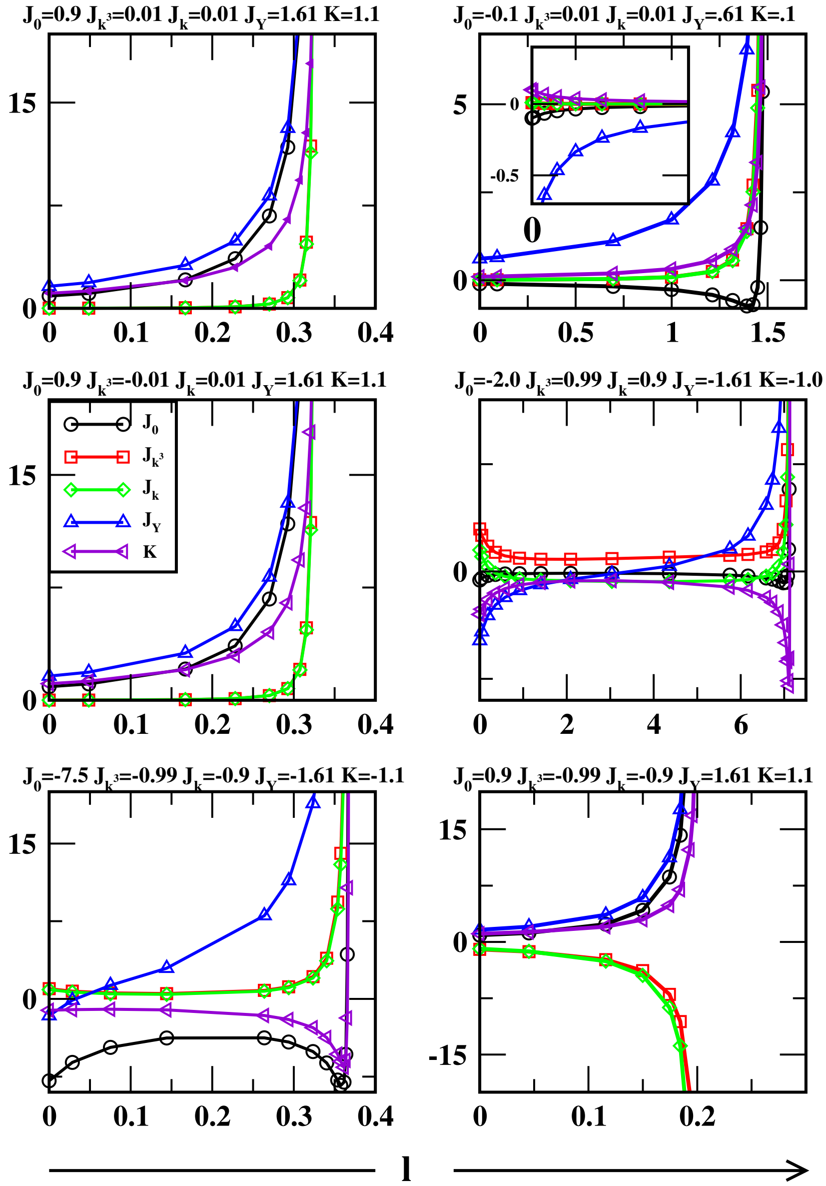

Figure 8: Numerical solutions of the RG equations (21) at the fixed points in the flow diagrams. The x-axis represents the flow parameter, and each plot is labeled with the initial conditions for the RG ODE evolution. Diverging solutions indicate strong coupling regimes, while abrupt sign-changing cusp-like features correspond to dissipative regimes. The inset graph corresponds to a large negative RKKY, whereas the remaining plots use small initial values for RKKY. The results illustrate that renormalizing RKKY requires contributions from all other bath-induced couplings, leading them to flow to zero.

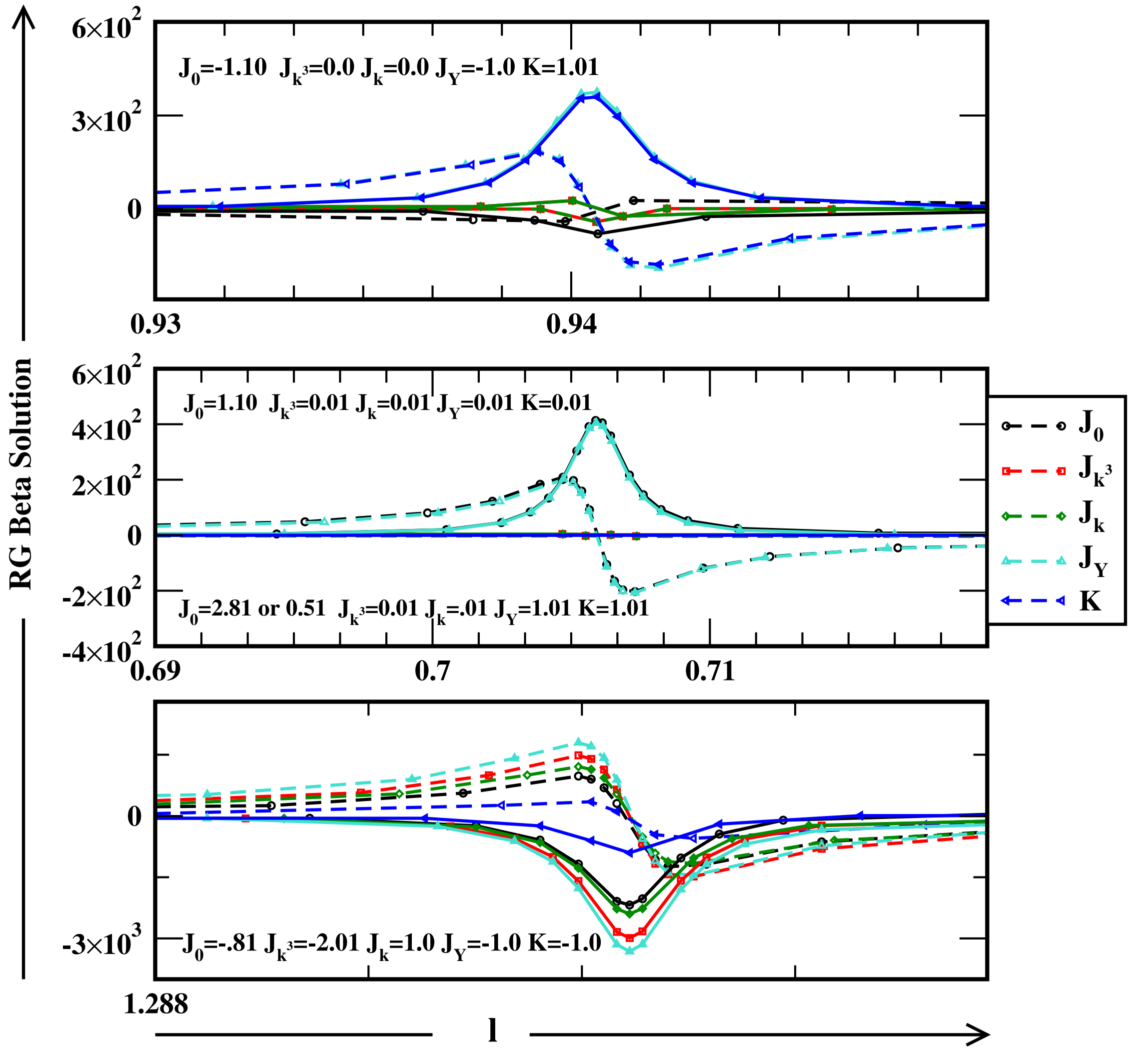

Figure 9: Dotted and thick lines correspond to real and imaginary coupling values, respectively. Sign reversion occurs in all couplings for imaginary weights at $J_{k^3} = -2.0$ in the bottom plot. The middle panel shows two initial conditions in one plot, with conditions labeled inside the figure. Between two sign-reversing phases (top to bottom), various two-pole and three-pole regimes emerge. We verified that sign reversion (SR) in imaginary weights occurs at these dissipative (spiral) fixed points for both one- and two-impurity cases.

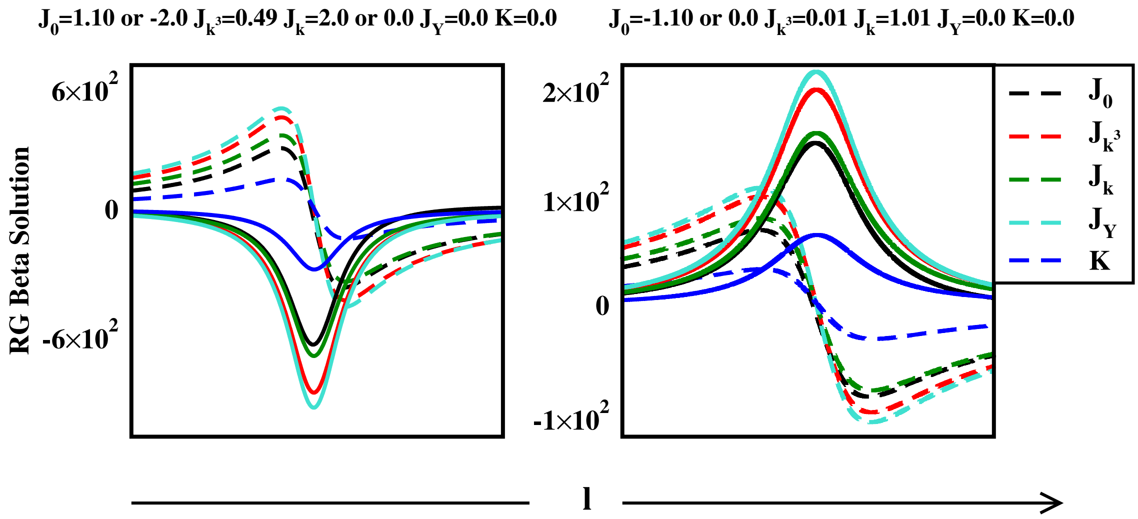

Figure 10: Sign reversion at the fixed points, particularly at the red points in Figure 7 (second row), compared to the unstable black point in the bottom row. The initial conditions for other couplings are set to very small values to ensure the one-impurity regime in equations 21.

8 Impurity Transport Calculation

We compute the anomalous contributions to the relaxation time in the presence of a non-linear dispersive bath using the $\mathcal{T}_{kk'}$ formalism [35], with detailed calculations provided in Appendix E. The expression for the relaxation time is given by:

$$\frac{1}{\tau} \propto (1 - 2J\tilde{g}_\alpha - 2J_{k^3}\tilde{g}_{\alpha k^3} - 2J_k\tilde{g}_{\alpha k}), \tag{24}$$

where the couplings J_0, J_k, J_{k^3} correspond to the bare model parameters, while the integrals $\tilde{g}_\alpha$, $\tilde{g}_{\alpha k^3}$, and $\tilde{g}_{\alpha k}$ arise from second-order perturbation theory (see Appendix E).

We further investigate the criticality associated with dissipative fixed points obtained from perturbative RG. Our analysis reveals two distinct scaling collapse regimes, as discussed in the next section, and an emergent invariant structure that persists in the RG flow.

8.1 Scaling Collapse in $\frac{1}{\tau}$

In the previous sections, we identified emergent coalescing points, which arise when the integrand vanishes in Eq. (58) or when $q \to 0$. These points are given by the condition

$$(k^2 - \mu)^2 - \lambda^2 k^2 = 0, \tag{25}$$

yielding momentum roots

$$\frac{k}{\lambda} = \frac{1}{2} \pm \frac{1}{2}\sqrt{1 + 4\frac{\mu}{\lambda^2}}. \tag{26}$$

We compare this to the RG-invariant relation,

$$J_k = \frac{1}{2} \pm \frac{1}{2}\sqrt{1 + 4mJ_{k^3}}, \tag{27}$$

noting that in the small β limit, the relations $J_k \propto \frac{k}{\lambda}$ and $J_{k^3} \propto \frac{1}{\lambda^2}$ hold, with μ corresponding to the invariant m. This analysis is reminiscent of the laser-induced Kondo effect studied in [41].

Exceptional points exist only when the chemical potential $\mu \neq 0$, marking a critical regime where null momentum points emerge. Beyond a critical value of μ, the system transitions to complex momentum values, signaling a complex gauge choice for momentum. These null momentum points also manifest in the diagonalization of the effective spin-spin Hamiltonian.

To illustrate these results, we plot the computed functions in Fig. 11, fixing $\mu = -1.0$ and $\lambda = 1.0$ while varying ϵ. We then rescale the functions and their arguments with the bandwidth, following the momentum roots prescription discussed earlier, to demonstrate scaling collapse. The scaling analysis can be extended to strong dissipation with complex-valued couplings, which is beyond the scope of this work. Here, we focus on establishing the emergence of an invariant structure induced by bath perturbations.

In the anisotropic model, scattering terms with $\mathcal{PC}$ symmetry give rise to a non-Hermitian Kondo problem. Under renormalization, special points (SPs) emerge, potentially exhibiting complex critical behavior. A deeper understanding of these effects may require specialized methods tailored to the specific nature of dissipation. Note that additional scattering terms were not included in our transport calculations; their impact on transport can be addressed in a separate study.

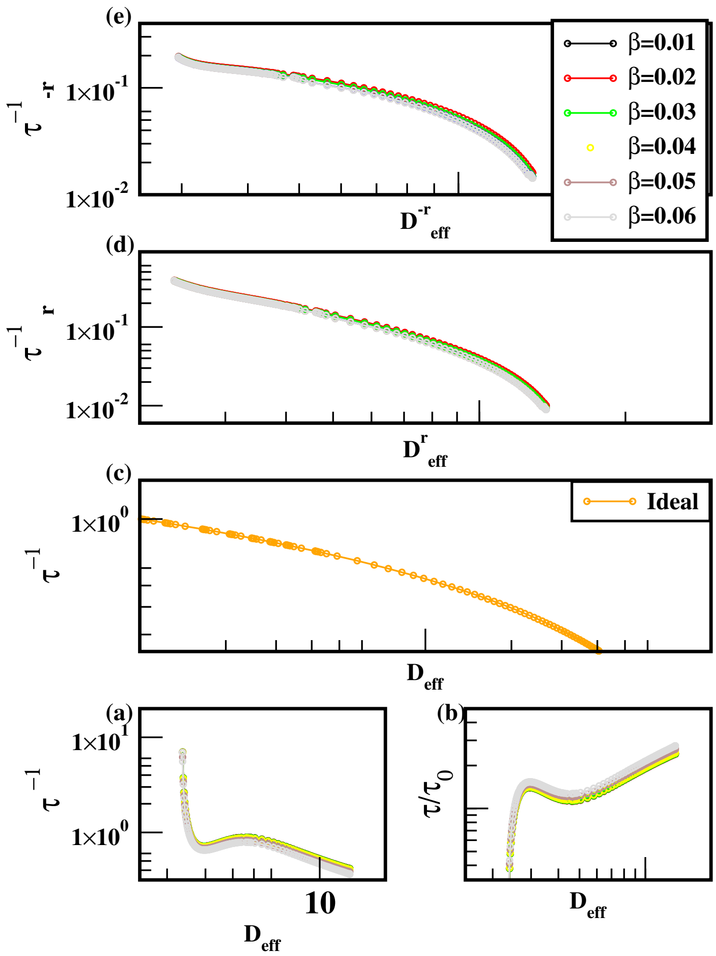

Figure 11: (a) Relaxation time τ for different values of the nonlinear parameter β, where τ^{-1} is proportional to resistivity. (b) The first point of each curve is scaled, showing a kink in τ. (c), (d) Scaling collapse is demonstrated, with the kink disappearing when scaling is applied from two different roots, given by $\tau_{\pm r}^{-1} = \tau^{-1} \times (1 \pm \sqrt{4D_{\text{eff}} + 1})$ and $D_{\text{eff}}^{\pm r} = D_{\text{eff}} \times (1 \pm \sqrt{4D_{\text{eff}} + 1})$.

9 Results and Discussion

The nontrivial renormalization of the impurity problem is demonstrated through the identification of dissipative fixed points in the model, revealed via perturbative renormalization group (RG) analysis incorporating $\mathcal{PC}$-symmetric potential scattering. In contrast to the well-known irrelevance of these terms under particle-hole symmetry, we find that $\mathcal{PC}$ interactions play a crucial role in the weak-to-intermediate interaction regime. Despite the presence of $\mathcal{PC}$ terms, a common invariant structure emerges in both RG analysis and relaxation-time calculations, governing the behavior of dissipative fixed points. Furthermore, we show that the local effective Hamiltonian for a single impurity undergoes a topological transition at the fixed points observed in the RG flow, reinforcing the importance of $\mathcal{PC}$-symmetric interactions in the problem. Additionally, we demonstrate that the high condition number of the local Hamiltonian in Fock space for real-valued couplings signals defectiveness, driven by anisotropy.

We analyze RG equations for single- and two-impurity problems in a homogeneous bath. Our results indicate that anisotropic $\mathcal{DM}$ interactions act as Hermiticity-breaking terms with $\mathcal{PC}$ symmetry, leading to the emergence of coalescing points in Kondo models. A distinctive transport signature arises due to residue contributions from a specific bath when $q \neq 0$. Numerical analysis of the RG flow diagrams reveals sign-reversion regimes at the fixed points, with potential scattering playing a crucial role in introducing openness to the system. As a result, these fixed points are specific to the type of dissipation considered. Furthermore, nonlinear perturbations contribute to the renormalization flow, with exceptional points appearing in the elliptic function solutions.

This study opens new avenues for experimentally realizing higher-order exceptional points and their associated topology in anisotropic vacancy-spin systems [21]. Exceptional points could also be realized in systems such as cavity-bath interactions and vacancy centers in diamond by controlling cubic perturbations. Our findings further motivate advanced Numerical Renormalization Group (NRG) calculations incorporating complex-valued and anisotropic $\mathcal{DM}$ interactions to investigate critical phenomena in dissipative quantum impurity models.

We also note that in our follow-up work using Keldysh mean-field Green functions, we observed similar fixed points and an intriguing hybridization evolution in non-equilibrium scenarios, particularly at exceptional points.

Acknowledgements

We thank JNCASR for the supportive research environment. Special thanks to Prof. Henrik Johannesson for conceptualizing the TKSS model, and to Prof. Ipsita Mandal and Dr. Ranjani Seshadri for introducing Weyl and topological systems. VMK acknowledges discussions with Alexander Poddubny on the NH skin effect in a Hermitian model.

10 appendix

10.1 Projection details for deriving effective sd model

The projection operator method is a versatile technique used in single-particle quantum mechanics [42] and many-body physics [35], particularly in the study of Kondo problems. It allows for the description of many-body wavefunctions in distinct sectors based on the occupancy of the impurity subspace, such as unoccupied (ψ_0), singly occupied (ψ_1), and doubly occupied (ψ_2) sectors. The method provides a formalism for projecting the total many-body wavefunction onto these sectors, facilitating a systematic analysis of the Kondo problem.

$$\Big(\sum_{i=0}^{2}|\psi_i\rangle\langle\psi_i|\Big)H\Big(\sum_{i=0}^{2}|\psi_i\rangle\langle\psi_i|\Big)\Big(\sum_{i=0}^{2}|\psi_i\rangle\langle\psi_i|\Big)\psi = E\Big(\sum_{i=0}^{2}|\psi_i\rangle\langle\psi_i|\Big)\psi \tag{28}$$

The identity operators can be represented as projectors onto the $(0,1,2)$ subspaces, corresponding to unoccupied, singly occupied, and doubly occupied states. These projectors are orthogonal.

$$\begin{gathered}\begin{pmatrix} H_{00} & H_{01} & H_{02} \\ H_{10} & H_{11} & H_{12} \\ H_{20} & H_{21} & H_{22} \end{pmatrix}\begin{pmatrix}\psi_0\\ \psi_1\\ \psi_2\end{pmatrix} = E\begin{pmatrix}\psi_0\\ \psi_1\\ \psi_2\end{pmatrix} \\ where\;\; P_\eta P_{\eta'} = \delta_{\eta\eta'}P_{\eta=\eta'}\;\; and\;\; P^I = P,\;\; I\in\mathcal{Z}^+ \\ H_{\eta,\eta'=0,1,2} = P_\eta H P_{\eta'}\end{gathered} \tag{29}$$

We can define the projection operators using impurity number operators satisfying the completness relation $\sum_\eta P_\eta = \mathcal{I}$ as $P_0 = (1-n_\downarrow)(1-n_\uparrow)$,$P_1 = n_\downarrow(1-n_\uparrow)+n_\uparrow(1-n_\downarrow)$, and $P_2 = n_\uparrow n_\downarrow$. The effective Hamiltonian for different subspaces can be obtained by eliminating the corresponding wave function in favor of the others.

$$H^{\eta}_{eff} = H_{\eta\eta} + \sum_{\substack{\eta'\neq\eta=0,1,2\\ \zeta,\zeta'=\pm}} H^{\zeta}_{\eta\eta'}\frac{1}{E-H_{\eta'\eta'}}H^{\zeta'}_{\eta'\eta} \tag{30}$$

In the equation 30, the index η and $\eta' = 0,1,2$ corresponds to the unoccupied, singly occupied, and doubly occupied states, respectively.Computing the P_1HP_2 we get the following,

$$\begin{aligned}\tilde{H}^{+}_{12} &= \sum_{k\theta}\tilde{V}^{\theta}_k\alpha_{k1}e^{-i\frac{\theta}{2}}c^{\dagger}_{k+}n_\downarrow d_\uparrow + \sum_{k\theta}e^{i\frac{\theta}{2}}\tilde{V}^{\theta}_k\alpha_{k2}c^{\dagger}_{k+}n_\uparrow d_\downarrow \\ \tilde{H}^{-}_{12} &= \sum_{k\theta}i\tilde{V}^{\theta}_k\alpha_{k2}e^{-i\frac{\theta}{2}}c^{\dagger}_{k-}n_\downarrow d_\uparrow - \sum_{k\theta}ie^{i\frac{\theta}{2}}\tilde{V}^{\theta}_k\alpha_{k1}c^{\dagger}_{k-}n_\uparrow d_\downarrow \\ \implies &(H^{+}_{21}+H^{-}_{21}) = (H^{+}_{12}+H^{-}_{12})^{\dagger}\end{aligned} \tag{31}$$

Similarly for the P_0HP_1 again only hybridization terms contribute can be shown as the following,

$$\begin{aligned}\tilde{H}^{+}_{10} &= \sum_{k\theta}\tilde{V}^{\theta}_k\alpha_{k1}e^{-i\frac{\theta}{2}}c^{\dagger}_{k+}(1-n_\downarrow)d_\uparrow + \sum_{k\theta}e^{i\frac{\theta}{2}}\tilde{V}^{\theta}_k\alpha_{k2}c^{\dagger}_{k+}(1-n_\uparrow)d_\downarrow \\ \tilde{H}^{-}_{10} &= \sum_{k\theta}i\tilde{V}^{\theta}_k\alpha_{k2}e^{-i\frac{\theta}{2}}c^{\dagger}_{k-}(1-n_\downarrow)d_\uparrow - \sum_{k\theta}ie^{i\frac{\theta}{2}}\tilde{V}^{\theta}_k\alpha_{k1}c^{\dagger}_{k-}(1-n_\uparrow)d_\downarrow \\ \implies &(H^{+}_{01}+H^{-}_{01}) = (H^{+}_{10}+H^{-}_{10})^{\dagger}\end{aligned} \tag{32}$$

The components H_{02} and H_{20} will vanish since P_0 commutes and also using the orthogonality $P_0P_2 = 0$. The remaining components can be computed as follows:

$$\begin{aligned}H_{00} &= \sum_{k\zeta}\epsilon_{k\zeta}c^{\dagger}_{k\zeta}c_{k\zeta}P_0 + \sum_{\sigma}\epsilon_d n_\sigma P_0, \\ H_{11} &= \sum_{k\zeta}\epsilon_{k\zeta}c^{\dagger}_{k\zeta}c_{k\zeta}P_1 + \sum_{\sigma}\epsilon_d n_\sigma P_1, \\ H_{22} &= \sum_{k\zeta}\epsilon_{k\zeta}c^{\dagger}_{k\zeta}c_{k\zeta}P_2 + \sum_{\sigma}\epsilon_d n_\sigma P_2 + Un_\uparrow n_\downarrow P_2.\end{aligned} \tag{33}$$

We will derive the components of the Hamiltonian to obtain the effective Hamiltonian can be expressed as:

$$H^1_{eff} = H_{11} + \sum_{\zeta,\zeta'=\pm} \left(H^{\zeta}_{12} \frac{1}{E - H_{22}} H^{\zeta'}_{21} + H^{\zeta}_{10} \frac{1}{E - H_{00}} H^{\zeta'}_{01} \right)$$

The derivation proceeds as follows:

$$\begin{aligned}
&\sum_{\zeta,\zeta'=\pm} H^{\zeta}_{12} \frac{1}{E - H_{22}} H^{\zeta'}_{21} \\
&= H^{+}_{12} \frac{1}{E - H_{22}} H^{+}_{21} + H^{+}_{12} \frac{1}{E - H_{22}} H^{-}_{21} + H^{-}_{12} \frac{1}{E - H_{22}} H^{+}_{21} + H^{-}_{12} \frac{1}{E - H_{22}} H^{-}_{21} \\
&= \sum_{kk'\theta\theta'} \tilde{V}^{\theta}_{k} \tilde{V}^{*\theta'}_{k'} \left(\alpha_{k1} e^{-i\frac{\theta}{2}} c^{\dagger}_{k+} n_{\downarrow} d_{\uparrow} + e^{i\frac{\theta}{2}} \alpha_{k2} c^{\dagger}_{k+} n_{\uparrow} d_{\downarrow} \right) \hat{M}_{22} \left(\alpha_{k'1} e^{-i\frac{\theta'}{2}} c^{\dagger}_{k'+} n_{\downarrow} d_{\uparrow} + e^{i\frac{\theta'}{2}} \alpha_{k'2} c^{\dagger}_{k'+} n_{\uparrow} d_{\downarrow} \right)^{\dagger} \\
&+ \sum_{kk'\theta\theta'} \tilde{V}^{\theta}_{k} \tilde{V}^{*\theta'}_{k'} \left(\alpha_{k1} e^{-i\frac{\theta}{2}} c^{\dagger}_{k+} n_{\downarrow} d_{\uparrow} + e^{i\frac{\theta}{2}} \alpha_{k2} c^{\dagger}_{k+} n_{\uparrow} d_{\downarrow} \right) \hat{M}_{22} \left(i\alpha_{k'2} e^{-i\frac{\theta'}{2}} c^{\dagger}_{k'-} n_{\downarrow} d_{\uparrow} - i e^{i\frac{\theta}{2}} \alpha_{k'1} c^{\dagger}_{k'-} n_{\uparrow} d_{\downarrow} \right)^{\dagger} \\
&+ \sum_{kk'\theta\theta'} \tilde{V}^{\theta}_{k} \tilde{V}^{*\theta'}_{k'} \left(i\alpha_{k2} e^{-i\frac{\theta}{2}} c^{\dagger}_{k-} n_{\downarrow} d_{\uparrow} - i e^{i\frac{\theta}{2}} \alpha_{k1} c^{\dagger}_{k-} n_{\uparrow} d_{\downarrow} \right) \hat{M}_{22} \left(\alpha_{k'1} e^{-i\frac{\theta'}{2}} c^{\dagger}_{k'+} n_{\downarrow} d_{\uparrow} + e^{i\frac{\theta'}{2}} \alpha_{k'2} c^{\dagger}_{k'+} n_{\uparrow} d_{\downarrow} \right)^{\dagger} \\
&+ \sum_{kk'\theta\theta'} \tilde{V}^{\theta}_{k} \tilde{V}^{*\theta'}_{k'} \left(i\alpha_{k2} e^{-i\frac{\theta}{2}} c^{\dagger}_{k-} n_{\downarrow} d_{\uparrow} - i e^{i\frac{\theta}{2}} \alpha_{k1} c^{\dagger}_{k-} n_{\uparrow} d_{\downarrow} \right) \hat{M}_{22} \left(i\alpha_{k'2} e^{-i\frac{\theta'}{2}} c^{\dagger}_{k'-} n_{\downarrow} d_{\uparrow} - i e^{i\frac{\theta'}{2}} \alpha_{k'1} c^{\dagger}_{k'-} n_{\uparrow} d_{\downarrow} \right)^{\dagger}
\end{aligned} \tag{34}$$

In equation 34 $\hat{M}_{22} = \frac{1}{E - H_{22}}$, we simplify using commutation algebra for operators of the form $\frac{1}{E - O_1} O_2$, where $[O_1, O_2] = cO_2$. This allows us to rewrite the expression as a power series and show explicit calculations for a specific component in H_{eff}.

$$\begin{aligned}
&\sum_{\zeta,\zeta'=\pm} H^{\zeta}_{10} \frac{1}{E - H_{00}} H^{\zeta'}_{01} \\
&= H^{+}_{10} \frac{1}{E - H_{00}} H^{+}_{01} + H^{+}_{10} \frac{1}{E - H_{00}} H^{-}_{01} + H^{-}_{10} \frac{1}{E - H_{00}} H^{+}_{01} + H^{-}_{10} \frac{1}{E - H_{00}} H^{-}_{01} \\
&= \sum_{kk'\theta\theta'} \tilde{V}^{\theta}_{k} \tilde{V}^{*\theta'}_{k'} \left(\alpha_{k1} e^{-i\frac{\theta}{2}} c^{\dagger}_{k+} \bar{n}_{\downarrow} d_{\uparrow} + e^{i\frac{\theta}{2}} \alpha_{k2} c^{\dagger}_{k+} \bar{n}_{\uparrow} d_{\downarrow} \right) \hat{M}_{00} \left(\alpha_{k'1} e^{-i\frac{\theta'}{2}} c^{\dagger}_{k'+} \bar{n}_{\downarrow} d_{\uparrow} + e^{i\frac{\theta'}{2}} \alpha_{k'2} c^{\dagger}_{k'+} \bar{n}_{\uparrow} d_{\downarrow} \right)^{\dagger} \\
&+ \sum_{kk'\theta\theta'} \tilde{V}^{\theta}_{k} \tilde{V}^{*\theta'}_{k'} \left(\alpha_{k1} e^{-i\frac{\theta}{2}} c^{\dagger}_{k+} \bar{n}_{\downarrow} d_{\uparrow} + e^{i\frac{\theta}{2}} \alpha_{k2} c^{\dagger}_{k+} \bar{n}_{\uparrow} d_{\downarrow} \right) \hat{M}_{00} \left(i\alpha_{k'2} e^{-i\frac{\theta'}{2}} c^{\dagger}_{k'-} \bar{n}_{\downarrow} d_{\uparrow} - i e^{i\frac{\theta}{2}} \alpha_{k'1} c^{\dagger}_{k'-} \bar{n}_{\uparrow} d_{\downarrow} \right)^{\dagger} \\
&+ \sum_{kk'\theta\theta'} \tilde{V}^{\theta}_{k} \tilde{V}^{*\theta'}_{k'} \left(i\alpha_{k2} e^{-i\frac{\theta}{2}} c^{\dagger}_{k-} \bar{n}_{\downarrow} d_{\uparrow} - i e^{i\frac{\theta}{2}} \alpha_{k1} c^{\dagger}_{k-} \bar{n}_{\uparrow} d_{\downarrow} \right) \hat{M}_{00} \left(\alpha_{k'1} e^{-i\frac{\theta'}{2}} c^{\dagger}_{k'+} \bar{n}_{\downarrow} d_{\uparrow} + e^{i\frac{\theta'}{2}} \alpha_{k'2} c^{\dagger}_{k'+} \bar{n}_{\uparrow} d_{\downarrow} \right)^{\dagger} \\
&+ \sum_{kk'\theta\theta'} \tilde{V}^{\theta}_{k} \tilde{V}^{*\theta'}_{k'} \left(i\alpha_{k2} e^{-i\frac{\theta}{2}} c^{\dagger}_{k-} \bar{n}_{\downarrow} d_{\uparrow} - i e^{i\frac{\theta}{2}} \alpha_{k1} c^{\dagger}_{k-} \bar{n}_{\uparrow} d_{\downarrow} \right) \hat{M}_{00} \left(i\alpha_{k'2} e^{-i\frac{\theta'}{2}} c^{\dagger}_{k'-} \bar{n}_{\downarrow} d_{\uparrow} - i e^{i\frac{\theta'}{2}} \alpha_{k'1} c^{\dagger}_{k'-} \bar{n}_{\uparrow} d_{\downarrow} \right)^{\dagger}
\end{aligned} \tag{35}$$

We consider $\theta = \theta'$ $k = k'$ for now, potential scattering will be included later. From equations

34 and 35, we derive the following component of the effective Hamiltonian.

$$
\begin{aligned}
H_{eff} &= H_{11} + \sum_{kk'\zeta}^{\theta\theta'} M_{kk'\zeta}^{\theta\theta'} \Big(e^{i\delta}\alpha_{k1}\alpha_{k'1}c_{k+}^{\dagger}d_{\uparrow}d_{\uparrow}^{\dagger}c_{k'+} + e^{-i\delta}\alpha_{k2}\alpha_{k'2}c_{k+}^{\dagger}d_{\downarrow}d_{\downarrow}^{\dagger}c_{k'+} + e^{i\phi}\alpha_{k2}\alpha_{k'1}c_{k+}^{\dagger}d_{\downarrow}d_{\uparrow}^{\dagger}c_{k'+} \\
&+ e^{-i\phi}\alpha_{k1}\alpha_{k2}c_{k+}^{\dagger}d_{\uparrow}d_{\downarrow}^{\dagger}c_{k'+}\Big) + i\sum_{kk'\zeta}^{\theta\theta'} M_{kk'\zeta}^{\theta\theta'} \Big(\alpha_{k1}\alpha_{k'1}e^{-i\phi}c_{k+}^{\dagger}d_{\uparrow}d_{\downarrow}^{\dagger}c_{k'-} - e^{-i\delta}\alpha_{k2}\alpha_{k'1}c_{k+}^{\dagger}d_{\uparrow}d_{\uparrow}^{\dagger}c_{k'-} \\
&+ e^{i\delta}\alpha_{k2}\alpha_{k'1}c_{k+}^{\dagger}d_{\downarrow}d_{\downarrow}^{\dagger}c_{k'-} - \alpha_{k2}\alpha_{k'2}e^{i\phi}c_{k+}^{\dagger}d_{\downarrow}d_{\uparrow}^{\dagger}c_{k'-}\Big) - i\sum_{kk'\zeta}^{\theta\theta'} M_{kk'\zeta}^{\theta\theta'} \Big(\alpha_{k1}\alpha_{k'1}e^{i\phi}c_{k-}^{\dagger}d_{\downarrow}d_{\uparrow}^{\dagger}c_{k'+} \\
&- e^{i\delta}\alpha_{k2}\alpha_{k'1}c_{k-}^{\dagger}d_{\uparrow}d_{\uparrow}^{\dagger}c_{k'+} + e^{-i\delta}\alpha_{k1}\alpha_{k'2}c_{k-}^{\dagger}d_{\downarrow}d_{\downarrow}^{\dagger}c_{k'+} - e^{-i\phi}\alpha_{k2}\alpha_{k'2}c_{k-}^{\dagger}d_{\uparrow}d_{\downarrow}^{\dagger}c_{k'+}\Big) \\
&+ \sum_{kk'\zeta}^{\theta\theta'} M_{kk'\zeta}^{\theta\theta'} \Big(e^{i\delta}\alpha_{k1}\alpha_{k'1}c_{k-}^{\dagger}d_{\downarrow}d_{\downarrow}^{\dagger}c_{k'-} - e^{-i\phi}\alpha_{k2}\alpha_{k'1}c_{k-}^{\dagger}d_{\uparrow}d_{\downarrow}^{\dagger}c_{k'-} - e^{i\phi}\alpha_{k1}\alpha_{k2}c_{k-}^{\dagger}d_{\downarrow}d_{\uparrow}^{\dagger}c_{k'-} \\
&+ e^{-i\delta}\alpha_{k2}\alpha_{k'2}c_{k-}^{\dagger}d_{\uparrow}d_{\uparrow}^{\dagger}c_{k'-}\Big)
\end{aligned}
\tag{36}
$$

where in above $\delta = \frac{\theta}{2} - \frac{\theta'}{2}$ and $\phi = \frac{\theta}{2} + \frac{\theta'}{2}$. It can be seen in above equation 36 $H_{eff} = H_{eff}^{\dagger}$ since the k, k' summations interchangeable.In equation 36 the elements $M_{kk'\zeta}^{\theta\theta'} = \frac{\tilde{V}_k^{\theta}\tilde{V}_{k'}^{\theta'}}{-\epsilon_d+\epsilon_{k\zeta}} + \frac{\tilde{V}_k^{\theta}\tilde{V}_{k'}^{\theta'}}{U+\epsilon_d-\epsilon_{k\zeta}}$ and $\tilde{V}_k^{\theta} = \frac{V_k}{\sqrt{\beta\gamma k^3\cos 3\theta}}$.we demonstrate how anisotropy arises in a Hermitian problem and its associated symmetry, leading to exceptional points. It's important to note that not all perturbative methods lead to exceptional points unless there are symmetries present even in the original model. In the current scenario, we have two crucial tuning parameters, denoted as k and θ, which significantly influence the local Hamiltonian properties. Additionally, the β parameter term plays a role similar to a magnetic field coupled system, such as $B * S_z$, except it is associated with dispersion in this particular problem.*Note that the edge contribution, which solely emerges in the cross-terms, particularly $\vec{s}\times\vec{S}_{kk'}$, does not contribute to $s_z S_{kk'}^z$. That is why the spin Hamiltonian in equation 16 show topological properties.*We simplify the above and use the Abrikosov representation [43] for spin for impurity as $s = \psi_d^{\dagger}\sigma\psi_d$ and $S_k = \psi_k^{\dagger}\sigma\psi_k$ for bath operators. In this representation, σ is the Pauli matrix, $\psi_d^{\dagger} = \begin{pmatrix} d_{\uparrow}^{\dagger} & d_{\downarrow}^{\dagger}\end{pmatrix}$ and $\psi_k^{\dagger} = \begin{pmatrix} c_{k\uparrow}^{\dagger} & c_{k'\downarrow}^{\dagger}\end{pmatrix}$. Collecting all terms in equation 36,

$$
\begin{aligned}
H_{eff}^{1} &= H_{11} + \sum_{kk'\zeta} M_{kk'\zeta}^{\theta\theta'} \Bigg((\alpha_{k1}\alpha_{k'1}e^{i\delta} + e^{-i\delta}\alpha_{k2}\alpha_{k'2}) s_z S_{kk'}^{z} \\
&+ (\alpha_{k1}\alpha_{k'1} + \alpha_{k2}\alpha_{k'2})\Big(e^{i\phi}s_- S_{kk'}^{+} + e^{-i\phi}S_{kk'}^{-}s_+ \Big) + \alpha_{k1}\alpha_{k'2}\underline{\underline{\big(e^{i\phi}s_- S_{kk'}^{z} + e^{-i\phi}S_{kk'}^{z}s_+ \big)}} \\
&+ \underline{i(\alpha_{k1}\alpha_{k'1} - \alpha_{k2}\alpha_{k'2})\Big(e^{i\phi}s_- S_{kk'}^{+} - e^{-i\phi}S_{kk'}^{-}s_+ \Big)} + \underline{\underline{\alpha_{k1}\alpha_{k'2}\Big(-ie^{i\delta}s_z S_{kk'}^{-} + ie^{-i\delta}S_{kk'}^{+}s_z \Big)}}\Bigg)
\end{aligned}
\tag{37}
$$

A simplification in doubly underlined terms leads to anisotropic $\mathcal{DM}$-interaction. For symmetry properties, refer to the section III in the main article.Substituting $\alpha_{k1} = \sqrt{\Delta + \beta k^3\cos 3\theta}$, $\alpha_{k'2} = \sqrt{\Delta - \beta(k')^3\cos 3\theta'}$ and in limit $k \to k'$ we get simplifications as $\alpha_{k1}^2 + \alpha_2^2 = \Delta$, where the $\Delta = \sqrt{\beta^2 k^6\cos^2 3\theta + \lambda^2 k^2}$, $\alpha_1^2 - \alpha_2^2 = \beta k^3\cos 3\theta$ and $\alpha_1\alpha_2 = k\lambda$.This model is then rewritten in the form of anisotropic $\mathcal{DM}$ interaction model as equation 10.Analyzing the prefactors of $M_{kk'}^{\theta\theta'}$, which scale as $\frac{V_k}{\sqrt{\beta\gamma k^3\cos 3\theta}}\frac{V_{k'}}{\sqrt{\beta\gamma(k')^3\cos 3\theta'}}$, we can consider the scatterings by constructing a regular hexagon, as the $\cos 3\theta$ takes maximum values at the points of this hexagonal cell. For any given k point at band edges, these scatterings will be high-energy states and need to be integrated out. As we discussed in the main article, we proceed by constructing the new spinor as $\psi^\dagger = \begin{pmatrix} c^\dagger_{k\frac{2\pi}{3}+} & c^\dagger_{k\frac{\pi}{3}-} & c^\dagger_{k-\frac{2\pi}{3}+} & c^\dagger_{k-\frac{\pi}{3}-} \end{pmatrix}$; in this basis, the Hamiltonian may be written in a more general form discussed in the next section.

11 Including the potential scattering

In the main article we discussed about the incorporated potential scattering terms, Here we expand model and detail how we can use the lie matrices algebra to compute RG equations. We can expand the above equation by expressing it in terms of magnitudes and operators in vector form, where the spin operator components are denoted with a hat symbol.

$$
\begin{aligned}
H^1_{eff} &= H_0 + \sum_{kk'} J_0\Big(S_x\hat{\Sigma}_x + S_y\hat{\Sigma}_y + S_z\hat{\Sigma}_z\Big) + i\sum_{kk'}|\vec{J}_{k^3}|(S_x\hat{\Sigma}_y - \hat{\Sigma}_x S_y) - \sum_{kk'}|\vec{g}_{1k^3}|(S_x\hat{\Omega}_y - \hat{\Omega}_x S_y) \\
&+ \sum_{kk'}|\vec{g}_{2k^3}|(S_x\hat{\Gamma}_y - \hat{\Gamma}_x S_y) + i\sum_{kk'}|\vec{J}_k|\Big((S_y\hat{\Sigma}_z - \hat{\Sigma}_y S_z) + (S_x\hat{\Sigma}_z - \hat{\Sigma}_x S_z)\Big) \\
&- \sum_{kk'}|\vec{g}_{1k}|\Big((S_y\hat{\Omega}_z - \hat{\Omega}_y S_z) + (S_x\hat{\Omega}_z - \hat{\Omega}_x S_z)\Big) + i\sum_{kk'}|\vec{g}_{2k}|\Big((S_y\hat{\Gamma}_z - \hat{\Gamma}_y S_z) + (S_x\hat{\Gamma}_z - \hat{\Gamma}_x S_z)\Big)
\end{aligned} \tag{38}
$$

We use the diagrams [44–47] with all permutations of vertices using the following algebra for third order perturbation theory,

$$
\begin{aligned}
[\Sigma_a, \Sigma_b] &= 4i\,\epsilon_{abc}\,\Sigma_c, \\
[\Sigma_a\Sigma_b, \Sigma_c] &= 8i\,\epsilon_{abc}\,\mathcal{I} - 8\,\delta_{ab}\,\Sigma_c + 8\,\delta_{ac}\,\Sigma_b, \\
[\Gamma_a, \Gamma_b] &= 4i\,\epsilon_{abc}\,\Gamma_c, \\
[\Gamma_a\Gamma_b, \Gamma_c] &= 8i\,\epsilon_{abc}\,\mathcal{I} - 8\,\delta_{ab}\,\Gamma_c + 8\,\delta_{ac}\,\Gamma_b, \\
[\Omega_a, \Omega_b] &= 4i\,\epsilon_{abc}\,\Omega_c, \\
[\Omega_a\Omega_b, \Omega_c] &= 8i\,\epsilon_{abc}\,\mathcal{I} - 8\,\delta_{ab}\,\Omega_c + 8\,\delta_{ac}\,\Omega_b, \\
[\Omega_a, \Sigma_b] &= 0, \\
[\Omega_a\Sigma_b, \Sigma_c] &= 4i\,\epsilon_{bcd}\begin{pmatrix} \sigma_a\sigma_d & \sigma_a\sigma_d \\ -\sigma_a\sigma_d & -\sigma_a\sigma_d \end{pmatrix}, \\
[\Sigma_a\Omega_b, \Gamma_c] &= 0.
\end{aligned} \tag{39}
$$

Where in above equation 39 $\Sigma_i = \begin{pmatrix} \sigma_i & \sigma_i \\ \sigma_i & \sigma_i \end{pmatrix}$, $\Omega_i = \begin{pmatrix} \sigma_i & 0 \\ 0 & -\sigma_i \end{pmatrix}$, $\Gamma_i = \begin{pmatrix} \sigma_i & 0 \\ 0 & \sigma_i \end{pmatrix}$ and $\Upsilon = \begin{pmatrix} \mathcal{I}_{2\times 2} & 0 \\ 0 & \mathcal{I}_{2\times 2} \end{pmatrix}$ these conventions used earlier [5]. The subscript i refers a,b and c which are Pauli matrices.Using the algebra we derive RG equations as follows,

$$
\begin{aligned}
\frac{dJ_0}{dl} &= J_0^2 + J_{k^3}^2 + J_k^2 + J_{k^3}J_k + J_k^2 J_0 + J_{k^3}^2 J_0 + J_0^3 - J_{k^3} g_{2k} - J_{k^3} g_{2k^3} - J_k g_{2k} + g_{2k}^2 J_{k^3} + g_{2k^3}^2 J_k - J_k^2 g_{2k^3} \\
\frac{dJ_{k^3}}{dl} &= J_k^2 + J_0 J_{k^3} + J_k^2 J_{k^3} + J_0^2 J_{k^3} + J_{k^3}^3, \quad \frac{dJ_k}{dl} = J_0 J_k + J_0^2 J_k + J_k J_{k^3}^2 + J_k^3 \\
\frac{dg_{1k^3}}{dl} &= g_{1k^3}^3 - g_{1k}^2 g_{1k^3}, \quad \frac{dg_{1k}}{dl} = g_{1k}^3 - g_{1k^2}^2 g_{1k} \\
\frac{dg_{2k^3}}{dl} &= -g_{2k^3}^3 + g_{1k^3}^2 g_{2k^3}, \quad \frac{dg_{2k}}{dl} = -g_{2k}^3 + g_{1k}^2 g_{2k}
\end{aligned}
\tag{40}
$$

From above, we identify various RG invariants as $\frac{g_{1k3}}{g_{1k}} = m_1$, and we can notice that after adding the potential scattering terms, we still have the invariant $J_k^2 + J_k = mJ_{k^3}$ and $\frac{g_{2k}^2(g_{2k}+\sqrt{m_2})}{(g_{2k}-\sqrt{m_2})} = \frac{g_{2k^3}^2(g_{2k^3}+\sqrt{m_2/m_1})}{(g_{2k^3}-\sqrt{m_2/m_1})}$

11.1 Analytic Solution of RG Equations

A straightforward simplification of the equations 11 for J_{k^3} and J_k by eliminating J_0 yields the following expressions:

$$
\frac{dJ_{k^3}}{dl} - J_k^2 = \frac{J_{k^3}}{J_k}\frac{dJ_k}{dl}, \frac{1}{J_{k^3}}\frac{dJ_{k^3}}{dl} - \frac{J_k^2}{J_{k^3}} = \frac{1}{J_k}\frac{dJ_k}{dl} \tag{41}
$$

By performing a substitution $\frac{J_k^2}{J_{k^3}} = x$, which results in $\frac{dx}{dl} = 2\frac{J_k}{J_{k^3}}\frac{dJ_k}{dl} - \frac{J_k^2}{J_{k^3}^2}\frac{dJ_{k3}}{dl}$, and subsequently rearranging the equation, we obtain the solution $J_k = \frac{1}{2} \pm \frac{1}{2}\sqrt{1+4mJ_{k^3}}$.We can derive the complete solution by variable separation as follows:

$$
J_0\frac{dJ_0}{dl} - J_0^3 = n, \left(\frac{J_k^2 + J_k}{m} + J_k\frac{(J_k+1)^2}{m^2} + J_k\right)\frac{dJ_k}{dl} = n \tag{42}
$$

The resulting solution will be in terms of two invariants, n and m. When we allow for complex solutions, we find that $J_k^* \to \frac{\sqrt{3}e^{i\frac{\pi}{3}}}{2}$, $J_{k^3}^* \to \frac{9e^{i\frac{\pi}{3}}}{16}$, and $m = e^{i\frac{\pi}{3}}$, with J_0^* having a $\tan^{-1}$ quantity that vanishes for $J_0^* = \pm 1$ in both ferromagnetic and antiferromagnetic cases as $n \to 1$. Please see equations in 43. Additionally, the logarithmic contribution to the scale vanishes when $J_0^* = -2$. These fixed points(complex) are obtained by incorporating the potential scattering terms.

$$
\log\left(\frac{[m^2 + m(J_k-1) + (J_k-1)^2]^{3\gamma}}{J_k^{2\gamma}}\right) + \frac{(m-2)}{\sqrt{3}(m^2-m+1)}\tan^{-1}\left(\frac{m+2J_k-2}{\sqrt{3}m}\right) = n\log D_{eff} \tag{43}
$$

Solving first equation in 42 for J_0 as following,

$$
\frac{\log\left(n^{2/3} + \sqrt[3]{n}(-J_0) + J_0^2\right) - 2\log\left(\sqrt[3]{n} + J_0\right)}{6\sqrt[3]{n}} \frac{-2\sqrt{3}\tan^{-1}\left(\frac{1-\frac{2J_0}{\sqrt[3]{n}}}{\sqrt{3}}\right)}{6\sqrt[3]{n}} = \log D_{eff} \tag{44}
$$

In above equation $\gamma = \frac{-m}{6*(m^2-m+1)}$ and gamma diverges when $m = e^{\pm i\frac{\pi}{3}}$.As a result we expect complex fixed points and as exponent γ diverge.

A noteworthy similarity exists between the RG equations for a single impurity in edge states and that of two impurities having $\mathcal{DM}$ interactions. To explore this connection, we address the two-impurity problem by simplifying the RG equations. We consider setting all couplings to zero, except for $J_0 \neq J_Y \neq K \neq 0$.

$$\frac{dJ_0}{dl} = J_0^2 + J_Y J_0 + K J_0, \frac{dJ_Y}{dl} = J_Y^2 + J_0^2 + K^2, \frac{dK}{dl} = K^2 + K J_Y. \tag{45}$$

By solving the equations for J_0 and K, we obtain the solution $J_0 = \frac{RK}{K-1}$, where R is a constant or an invariant under renormalization. Using this solution, we proceed to solve for J_Y and K as follows:

$$J_Y \frac{dJ_Y}{dl} - J_Y^3 = R_1, \frac{dK}{dl} - K^2 = \frac{R_1}{\frac{R^2 K}{(1-K)^2} + K} \tag{46}$$

Solution to the J_Y equation can be written as follows:

$$\frac{\sqrt[3]{R_1}(-J_Y) + J_Y^2 + R_1^{2/3}}{(J_Y + \sqrt[3]{R_1})^2} e^{2\sqrt{3}\tan^{-1}\left(\frac{\frac{2J_Y}{\sqrt[3]{R_1}}-1}{\sqrt{3}}\right)} = D_{eff}^{6R_1^{\frac{1}{3}}} \tag{47}$$

For K-equation has higher order nonlinearity so we have solutions in two limits,

$$\begin{aligned} &\frac{\left(\sqrt[3]{R_1}(-K) + K^2 + R_1^{2/3}\right)}{\left(K + \sqrt[3]{R_1}\right)^2} e^{+2\sqrt{3}\tan^{-1}\left(\frac{\frac{2K}{\sqrt[3]{R_1}}-1}{\sqrt{3}}\right)} = D_{eff}^{6\sqrt[3]{R_1}}, \quad \text{for } K \to \infty \\ &\frac{-\frac{R^2}{K-1} + R^2 \log(K-1) + \frac{1}{2}(K-1)^2 + K}{R_1} = \log D_{eff}, \quad \text{for } K \to 0 \end{aligned} \tag{48}$$

In a similar fashion, we will work on solving the J_0 equation with J_Y in order to separate the solutions. For $R = R_1 = 1.0$, we will illustrate the RG flow in figure 12. We anticipate fixed points in different quadrants based on the sign chosen for these constants.

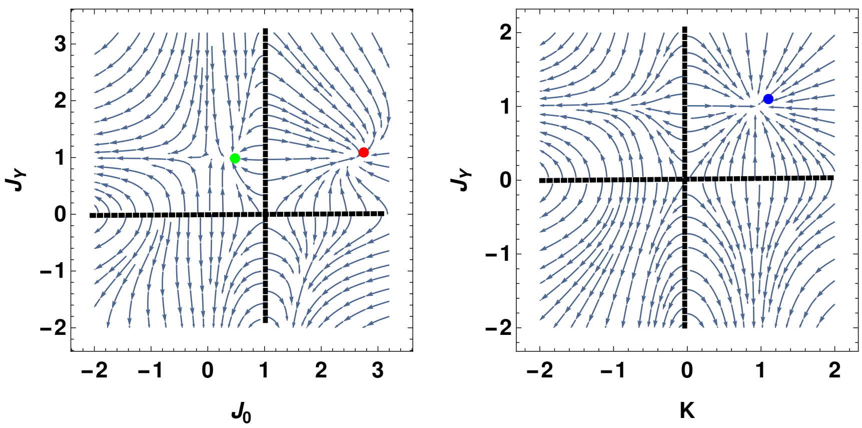

Figure 12: RG flow of two impurity show the FP can be in different quadrants with $R_1 = -1$ and $R = 1.0$. We get around the SP(($J_Y = 1.0, J_0 = 3.0$)) existing SR regime in couplings.

11.2 RKKY Interaction

The RKKY interaction in the edge states can be expressed by expanding it in the Fourier series for the spins.

$$J_Y(r_i - r_j) \propto \sum_{kk'hh'} \frac{V_{ij}}{\epsilon_{kh} - \epsilon_{k'h'}} e^{ik(r_i - r_j)} V^*_{ij} e^{-ik'(r_i - r_j)} = \int_0^{2\pi} \int_0^{\pi} \int_0^{k_f} \frac{k^2 sin\theta e^{ikR} dk d\theta d\phi}{\sqrt{k^6\beta^2 \cos^2 3\theta + \lambda^2 k^2}}$$
$$+ (k \neq k', h = h') \text{ terms} \tag{49}$$

We solve the above integral using the same method as in the impurity transport sections. We find that the leading contribution for J_Y can be expressed as the sum of special functions, given by $E_1(\epsilon) + E_2(\epsilon)$. With the substitution $\cos\theta = t$, we obtain the following expression.We don't set $\epsilon_k = \epsilon_{k'}$ as in the Poorman limit. Instead, we consider a chemical potential so that the integral does not diverge in this limit.

$$J_Y \propto \pi \int_k \frac{e^{ikR}}{k\beta} \oint \frac{q\, dt}{q^2 - (4t^3 - 3t)^2} + \sum_{kk'} \frac{|V_{ij}|}{k^2 - (k')^2} e^{ikr} e^{-ik'r},$$
$$\text{where} \quad q = \frac{\sqrt{(k^2-\mu)^2 - k^2}}{\beta k^3} \tag{50}$$

The distinct contribution from the conventional flat band occurs when $q \neq 0$. Vanishing points for momentum or bandwidth occur at two limits: as $\beta \to \infty$ or $\frac{k}{\lambda} \to \frac{1}{2} \pm \frac{1}{2}\sqrt{1 + 4\frac{\mu}{\lambda^2}}$, with $\mu = -0.25$ as a critical value for RKKY when $\lambda = 1.0$. The second term is a standard component in various studies and can be expressed using Bessel functions [48] or elliptic functions [49]. The first term can be expressed as a sum of odd and even parts; all the odd terms can be represented using elliptic functions and the even terms are composed of transcendental functions.

12 Impurity Transport Calculation

We follow the $\mathcal{T}_{kk'}$ formalism for the effective Kondo model in equation 10 to compute the relaxation time as follows,

$$\frac{1}{\tau} \propto \left(1 - 2J\tilde{g}_\zeta - 2J_{k^3}\tilde{g}_{\zeta k^3} - 2J_k \tilde{g}_{\zeta k}\right) \tag{51}$$

Where the ζ correspond to chiral index and takes vales $\zeta = \pm$ for each bands in effective model bands.

$$\tilde{g}_\zeta = \int_0^{2\pi} \int_0^{\pi} \int_0^{k_f} \frac{k^2 sin\theta dk d\theta d\phi}{k^2 + \zeta\sqrt{k^6\beta^2 \cos^2 3\theta + \lambda^2 k^2} - \mu} \tag{52}$$

where Solving the θ integral first, we get two pieces as follows,

$$\tilde{g}_\zeta = 2\pi \int_k k^2 \oint \frac{dt}{k^2 + \zeta\sqrt{k^6\beta^2(4t^3 - 3t)^2 + \lambda^2 k^2} - \mu} \tag{53}$$

we rationalize the above integral and write as the following by introducing $q = \frac{\sqrt{(k^2-\mu)^2 - \lambda^2 k^2}}{\beta k^3}$,

$$\tilde{g}_\zeta = 2\pi \int_k \frac{1}{k} \oint \frac{q + \bar{\zeta}\sqrt{(4t^3 - 3t)^2 + \frac{\lambda^2}{\beta^2 k^4}}dt}{q^2 - (4t^3 - 3t)^2} = \int_k \frac{\pi}{kq}\left(\sum_{res} f(t, q) + \sum_{res} f(t, -q)\right) \tag{54}$$

For finding these residues, we will use the roots of the cubic equations $\beta(4t^3-3t)\pm q=0$. We collect positive q roots and negative as follows for doing contour integrals,

$$t^{\zeta}=\begin{cases}\frac{1}{2}\left(\sqrt[3]{\sqrt{q^2-1}+\zeta q}+\frac{1}{\sqrt[3]{\sqrt{q^2-1}+\zeta q}}\right), \\ -\frac{1}{4}\left(1-i\sqrt{3}\right)\sqrt[3]{\sqrt{q^2-1}+\zeta q}-\frac{1+i\sqrt{3}}{4\sqrt[3]{\sqrt{q^2-1}+\zeta q}} \\ -\frac{1}{4}\left(1+i\sqrt{3}\right)\sqrt[3]{\sqrt{q^2-1}+\zeta q}-\frac{1-i\sqrt{3}}{4\sqrt[3]{\sqrt{q^2-1}+\zeta q}}\end{cases} \tag{55}$$

Where in above we have $\zeta=\pm$, Similarly, the other contributions are as follows,

$$\begin{aligned}\tilde{g}_{\zeta k^3}&=2\pi\beta\int_k k^2\oint\frac{((4t^3-3t)^2)(q+\bar{\zeta}r)}{q^2-(4t^3-3t)^2}dt, \tilde{g}_{\zeta k}=\int_k\oint\frac{(q+\bar{\zeta}r)}{q^2-(4t^3-3t)^2}dt \\ \text{where } r&=\sqrt{(4t^3-3t)^2+\frac{\lambda^2}{\beta^2k^4}}\end{aligned} \tag{56}$$

after summing over the $\zeta=\pm$ bands we get following simplifications,

$$\tilde{g}=2\pi\int_k\frac{1}{k}\oint\frac{qdt}{q^2-(4t^3-3t)^2}, \tilde{g}_{k^3}=2\pi\beta\int_k k^2\oint\frac{(4t^3-3t)^2qdt}{q^2-(4t^3-3t)^2}, \tilde{g}_k=\int_k\oint\frac{qdt}{q^2-(4t^3-3t)^2} \tag{57}$$

After contour integrals each contributes as $\oint\frac{qdt}{q^2-(4t^3-3t)^2}=q$ hence sum of all g_ζ contribution as following,

$$\tilde{g}(\mu)=\int(\beta qk^2-\beta q^4k+\frac{q}{k}-q)dk \tag{58}$$

We set $\epsilon\approx k^2$ and the density of states in 3D as $\rho(\epsilon)\approx\sqrt{\epsilon}$ then above integral yields,

$$\tilde{g}(\mu)=\int\left(\frac{\sqrt{(\epsilon-\mu)^2-\lambda^2\epsilon}}{\sqrt{\epsilon}}-\frac{((\epsilon-\mu)^2-\lambda^2\epsilon)^2}{\beta^3\epsilon^{6-\frac{1}{2}}}+\frac{\sqrt{(\epsilon-\mu)^2-\lambda^2\epsilon}}{\beta\epsilon^2}-\frac{\sqrt{(\epsilon-\mu)^2-\lambda^2\epsilon}}{\beta\epsilon^{\frac{3}{2}}}\right)d\epsilon \tag{59}$$

Where in above μ is the chemical potential can take any values around Fermi energy. We perform this above integral exactly in terms of special functions to extract contribution to $\frac{1}{\tau}$, which indeed scales with RG invariant in the elliptic functions.

$$
\begin{aligned}
&\tilde{g}_\epsilon \propto \frac{P_1(\epsilon)+P_{\frac{3}{2}}(\epsilon)+T_1(\epsilon)+E_1(\epsilon)+E_2(\epsilon)+\log(\epsilon)}{\beta^3}\\
&P_1(\epsilon) = -\frac{3\mu^4-16\mu^3\epsilon+4\mu^2\epsilon(9\epsilon-2)+2\epsilon^2\left(2\epsilon\left(\beta^2\sqrt{(\mu-\epsilon)^2-\epsilon}\left(2\sqrt{\epsilon}(\beta-\beta\epsilon+3)+3\right)-6\right)+3\right)}{12\epsilon^4}\\
&P_{\frac{3}{2}}(\epsilon) = \frac{8\mu\epsilon^2\left(2\beta^3\epsilon^{3/2}\sqrt{(\mu-\epsilon)^2-\epsilon}-6\epsilon+3\right)}{12\epsilon^4}\\
&T_1(\epsilon) = \beta^2\tanh^{-1}\left(\frac{-2\mu+2\epsilon-1}{2\sqrt{(\mu-\epsilon)^2-\epsilon}}\right)+\frac{(2\mu+1)\beta^2\coth^{-1}\left(\frac{2\mu\sqrt{(\mu-\epsilon)^2-\epsilon}}{2\mu(\mu-\epsilon)-\epsilon}\right)}{2\mu}\\
&E_1(\epsilon) = \frac{i\beta^2\epsilon\sqrt{\frac{-2\mu+\sqrt{4\mu+1}+2\epsilon-1}{\epsilon}}\sqrt{-\frac{2\mu+\sqrt{4\mu+1}-2\epsilon+1}{\epsilon}}\left(AE\left(i\sinh^{-1}\left(\frac{\sqrt{-2\mu-\sqrt{4\mu+1}-1}}{\sqrt{2}\sqrt{\epsilon}}\right)|\frac{2\mu-\sqrt{4\mu+1}+1}{2\mu+\sqrt{4\mu+1}+1}\right)\right)}{3\sqrt{2}\sqrt{-2\mu-\sqrt{4\mu+1}-1}\sqrt{(\mu-\epsilon)^2-\epsilon}}\\
&A = \left(2\mu+\sqrt{4\mu+1}+1\right)(2\mu\beta+\beta+6)\\
&E_2(\epsilon) = -\frac{B\left(\left(\sqrt{4\mu+1}+2\mu\left(\sqrt{4\mu+1}+2\right)+1\right)\beta+6\sqrt{4\mu+1}\right)F\left(i\sinh^{-1}\left(\frac{\sqrt{-2\mu-\sqrt{4\mu+1}-1}}{\sqrt{2}\sqrt{\epsilon}}\right)|\frac{2\mu-\sqrt{4\mu+1}+1}{2\mu+\sqrt{4\mu+1}+1}\right)}{3\sqrt{2}\sqrt{-2\mu-\sqrt{4\mu+1}-1}\sqrt{(\mu-\epsilon)^2-\epsilon}}\\
&B = i\beta^2\epsilon\sqrt{\frac{-2\mu+\sqrt{4\mu+1}+2\epsilon-1}{\epsilon}}\sqrt{-\frac{2\mu+\sqrt{4\mu+1}-2\epsilon+1}{\epsilon}}
\end{aligned}
\tag{60}
$$

In the above solution, F is an incomplete elliptic function of the first kind, and E is an elliptic function of the second kind. P and T are polynomial and transcendental functions, respectively.

References

[1] H.-P. Breuer, F. Petruccione *et al.*, *The theory of open quantum systems*, Oxford University Press on Demand (2002).

[2] Y. Ashida, Z. Gong and M. Ueda, *Non-hermitian physics*, Advances in Physics **69**(3), 249 (2020).

[3] F. Thompson and A. Kamenev, *Field theory of many-body lindbladian dynamics*, Annals of Physics **455**, 169385 (2023).

[4] M. Nakagawa, N. Kawakami and M. Ueda, *Non-hermitian kondo effect in ultracold alkaline-earth atoms*, Phys. Rev. Lett. **121**, 203001 (2018), doi:10.1103/PhysRevLett.121.203001.

[5] J. A. S. Lourenço, R. L. Eneias and R. G. Pereira, *Kondo effect in a $\mathcal{PT}$-symmetric non-hermitian hamiltonian*, Phys. Rev. B **98**, 085126 (2018), doi:10.1103/PhysRevB.98.085126.

[6] A. G. Shnirman, B. A. Malomed and E. Ben-Jacob, *Nonperturbative studies of a quantum higher-order nonlinear schrödinger model using the bethe ansatz*, Phys. Rev. A **50**, 3453 (1994), doi:10.1103/PhysRevA.50.3453.

[7] Y. O. Nakai, N. Okuma, D. Nakamura, K. Shimomura and M. Sato, *Topological enhancement of nonnormality in non-hermitian skin effects*, Phys. Rev. B **109**, 144203 (2024), doi:10.1103/PhysRevB.109.144203.

[8] P. Kattel, Y. Tang, J. H. Pixley and N. Andrei, *The kondo effect in the quantum xx spin chain*, Journal of Physics A: Mathematical and Theoretical (2024).

[9] P. Kattel, A. Zhakenov, P. R. Pasnoori, P. Azaria and N. Andrei, *Dissipation driven phase transition in the non-hermitian kondo model*, arXiv preprint arXiv:2402.09510 (2024).

[10] P. Kattel, P. R. Pasnoori, J. Pixley and N. Andrei, *A spin chain with non-hermitian pt- symmetric boundary couplings: exact solution, dissipative kondo effect, and phase transitions on the edge*, arXiv preprint arXiv:2406.10334 (2024).

[11] J. Li, M. Turaev, M. Matsubara, K. Kliemt, C. Krellner, S. Pal, M. Fiebig and J. Kroha, *Discovery of a non-hermitian phase transition in a bulk condensed-matter system* (2024), 2412.16012.

[12] T. Dai, Y. Ao, J. Mao, Y. Yang, Y. Zheng, C. Zhai, Y. Li, J. Yuan, B. Tang, Z. Li *et al.*, *Non-hermitian topological phase transitions controlled by nonlinearity*, Nature Physics **20**(1), 101 (2024).

[13] J. Chen, *Critical behavior of non-hermitian kondo effect in a pseudogap system*, Phys. Rev. B **111**, 045124 (2025), doi:10.1103/PhysRevB.111.045124.

[14] S. Han, D. J. Schultz and Y. B. Kim, *Complex fixed points of the non-hermitian kondo model in a luttinger liquid*, Phys. Rev. B **107**, 235153 (2023), doi:10.1103/PhysRevB.107.235153.

[15] V. M. Kulkarni, A. Gupta and N. S. Vidhyadhiraja, *Kondo effect in a non-hermitian $\mathcal{PT}$-symmetric anderson model with rashba spin-orbit coupling*, Phys. Rev. B **106**, 075113 (2022), doi:10.1103/PhysRevB.106.075113.

[16] K. Yamamoto, M. Nakagawa and N. Kawakami, *Correlation versus dissipation in a non-hermitian anderson impurity model*, arXiv preprint arXiv:2408.03494 (2024).

[17] P. Kumar and R. Bhatt, *Anisotropic quantum hall states in the presence of interactions with fourfold rotational symmetry*, Physical Review B **104**(3), 035147 (2021).

[18] C. Han and Z. Liu, *Anisotropy and quench dynamics of quasiholes in fractional quantum hall liquids*, Physical Review B **105**(4), 045108 (2022).

[19] T. Thakur and B. Szafran, *Vortex structure in wigner molecules*, Scientific Reports **13**(1), 1 (2023).

[20] A. N. Poddubny, *Interaction-induced analog of a non-hermitian skin effect in a lattice two-body problem*, Phys. Rev. B **107**, 045131 (2023), doi:10.1103/PhysRevB.107.045131.

[21] Y. Wu, Y. Wang, X. Ye, W. Liu, Z. Niu, C.-K. Duan, Y. Wang, X. Rong and J. Du, *Third-order exceptional line in a nitrogen-vacancy spin system*, Nature Nanotechnology **19**(2), 160 (2024).

[22] T. Isobe, T. Yoshida and Y. Hatsugai, *Bulk-edge correspondence for nonlinear eigenvalue problems*, Phys. Rev. Lett. **132**, 126601 (2024), doi:10.1103/PhysRevLett.132.126601.

[23] B. Zhen, C. W. Hsu, Y. Igarashi, L. Lu, I. Kaminer, A. Pick, S.-L. Chua, J. D. Joannopoulos and M. Soljačić, *Spawning rings of exceptional points out of dirac cones*, Nature **525**(7569), 354 (2015).

[24] J. Betancourt, S. Li, X. Dang, J. Burton, E. Tsymbal and J. Velev, *Complex band structure of topological insulator bi2se3*, Journal of Physics: Condensed Matter **28**(39), 395501 (2016).

[25] C.-X. Liu, X.-L. Qi, H. Zhang, X. Dai, Z. Fang and S.-C. Zhang, *Model hamiltonian for topological insulators*, Phys. Rev. B **82**, 045122 (2010), doi:10.1103/PhysRevB.82.045122.

[26] I. Boettcher, *Interplay of topology and electron-electron interactions in rarita-schwinger-weyl semimetals*, Phys. Rev. Lett. **124**, 127602 (2020), doi:10.1103/PhysRevLett.124.127602.

[27] H. Zhang, C.-X. Liu, X.-L. Qi, X. Dai, Z. Fang and S.-C. Zhang, *Topological insulators in bi2se3, bi2te3 and sb2te3 with a single dirac cone on the surface*, Nature physics **5**(6), 438 (2009).

[28] H.-F. Lü, Y.-H. Deng, S.-S. Ke, Y. Guo and H.-W. Zhang, *Quantum impurity in topological multi-weyl semimetals*, Phys. Rev. B **99**, 115109 (2019), doi:10.1103/PhysRevB.99.115109.

[29] A. K. Mitchell and L. Fritz, *Signatures of weyl semimetals in quasiparticle interference*, Phys. Rev. B **93**, 035137 (2016), doi:10.1103/PhysRevB.93.035137.

[30] M. Zarea, S. E. Ulloa and N. Sandler, *Enhancement of the kondo effect through rashba spin-orbit interactions*, Phys. Rev. Lett. **108**, 046601 (2012), doi:10.1103/PhysRevLett.108.046601.

[31] D. Mastrogiuseppe, A. Wong, K. Ingersent, S. E. Ulloa and N. Sandler, *Kondo effect in graphene with rashba spin-orbit coupling*, Phys. Rev. B **90**, 035426 (2014), doi:10.1103/PhysRevB.90.035426.

[32] M. Zarea and N. Sandler, *Rashba spin-orbit interaction in graphene and zigzag nanoribbons*, Phys. Rev. B **79**, 165442 (2009), doi:10.1103/PhysRevB.79.165442.

[33] R. Žitko, *Quantum impurity on the surface of a topological insulator*, Phys. Rev. B **81**, 241414 (2010), doi:10.1103/PhysRevB.81.241414.

[34] P. Delplace, T. Yoshida and Y. Hatsugai, *Symmetry-protected multifold exceptional points and their topological characterization*, Phys. Rev. Lett. **127**, 186602 (2021), doi:10.1103/PhysRevLett.127.186602.

[35] A. C. Hewson, *The Kondo problem to heavy fermions*, vol. 2, Cambridge university press (1997).

[36] A. Melkani, *Degeneracies and symmetry breaking in pseudo-hermitian matrices*, Phys. Rev. Res. **5**, 023035 (2023), doi:10.1103/PhysRevResearch.5.023035.

[37] A. Van der Sluis, *Condition numbers and equilibration of matrices*, Numerische Mathematik **14**(1), 14 (1969).

[38] D. F. Mross and H. Johannesson, *Two-impurity kondo model with spin-orbit interactions*, Phys. Rev. B **80**, 155302 (2009), doi:10.1103/PhysRevB.80.155302.

[39] B. A. Jones and C. M. Varma, *Study of two magnetic impurities in a fermi gas*, Phys. Rev. Lett. **58**, 843 (1987), doi:10.1103/PhysRevLett.58.843.

[40] B. A. Jones, C. M. Varma and J. W. Wilkins, *Low-temperature properties of the two-impurity kondo hamiltonian*, Phys. Rev. Lett. **61**, 125 (1988), doi:10.1103/PhysRevLett.61.125.

[41] M. Nakagawa and N. Kawakami, *Laser-induced kondo effect in ultracold alkaline-earth fermions*, Phys. Rev. Lett. **115**, 165303 (2015), doi:10.1103/PhysRevLett.115.165303.

[42] J. J. Sakurai, *Advanced quantum mechanics*, Pearson Education India (2006).

[43] A. A. Abrikosov, *Electron scattering on magnetic impurities in metals and anomalous resistivity effects*, Physics Physique Fizika **2**, 5 (1965), doi:10.1103/PhysicsPhysiqueFizika.2.5.

[44] S. Han, D. J. Schultz and Y. B. Kim, *Non-fermi liquid behavior and quantum criticality in cubic heavy fermion systems with non-kramers multipolar local moments*, Phys. Rev. B **106**, 155155 (2022), doi:10.1103/PhysRevB.106.155155.

[45] I. Affleck and A. W. Ludwig, *Exact conformal-field-theory results on the multichannel kondo effect: single-fermion green's function, self-energy, and resistivity*, Physical Review B **48**(10), 7297 (1993).

[46] P. Anderson, *A poor man's derivation of scaling laws for the kondo problem*, Journal of Physics C: Solid State Physics **3**(12), 2436 (1970).

[47] J. Sólyom, *Renormalization and scaling in the x-ray absorption and kondo problems*, Journal of Physics F: Metal Physics **4**(12), 2269 (1974).

[48] K. Szałowski and T. Balcerzak, *Rkky interaction with diffused contact potential*, Phys. Rev. B **78**, 024419 (2008), doi:10.1103/PhysRevB.78.024419.

[49] S. Okui, *Complete elliptic integrals resulting from integrals of bessel functions*, Journal of Research of the National Bureau of Standards: Mathematical sciences. B p. 113 (1974).